ABSTRACT

GRISSETT, GREGORY AARON. Three Dimensional Structures from Nonwovens. (Under the Direction of Behnam Pourdeyhimi.)

The purpose of this research was to assess molding or thermoforming nonwoven webs into a *three-dimensional fiber network* without the use of resin or binders via the SpaceNet Formed Fiber System ®. We define this network as a deep-draw structure with projections and/or depressions rising from an initial plane, providing a grid-domed structure. The research is comprised of three experimental components: the first concerned with moldability of nonwovens on the SpaceNet System. The second component comprised an evaluation of the effect process parameters on substrate deformation, and the third concerned with an investigation the effect of mold geometry on compressive properties.

Concerning the moldability of nonwovens, eight-nonwoven webs (six spunbond, two hydroentangled) were processed using the SpaceNet formed fiber system. Nonwovens comprised of a uniform fiber orientation and isotropic mechanical properties were found to process more efficiently in the SpaceNet system. Given this conclusion, spunbond nonwovens were selected for the remainder of the research described herein.

Different mold geometries were used to make three-dimensional structures from spunbond nonwovens and their respective compressive properties were evaluated. It was observed that decreases in pin diameter increased the compressive stress in all samples produced. It was also found that compressive resilience is not necessarily associated with changes in mold geometry but rather inherent fabric properties i.e. stiffness and level of bonding.

The effect of preheating and temperature on formed product dimensions was also evaluated. A split-plot factorial design was used and it was determined that temperature alone influences maximum deformation. Preheating (residence time) was observed to be insignificant including all interactions.

THREE DIMENSIONAL STRUCTURES FROM NONWOVENS

By

GREGORY AARON GRISSETT

A thesis submitted to the Graduate Faculty of
North Carolina State University
in partial fulfillment of the
requirements for the Degree of
Master of Science

TEXTILE MANAGEMENT AND TECHNOLOGY

Raleigh

2003

APPROVED BY:

_____ _____

_____
Chair of Advisory Committee

DEDICATION

This thesis is dedicated to my mother, Amelia Grissett, and father, James Phillip Grissett.

BIOGRPAHY

Gregory Aaron Grissett was born in Lawton, Oklahoma on September 20, 1978. After several moves, Gregory and his family moved to Jacksonville, NC where his parents now reside. Upon graduating from Jacksonville High School in 1996, Gregory enrolled in the College of Textiles at North Carolina State University. In December of 2000, Gregory graduated Magna Cum Laude with a Bachelors of Science degree in Textile Technology. Upon completion of his undergraduate work, Gregory entered the graduate program in Textile Management and Technology at the College of Textiles. During his graduate studies, Gregory completed an internship with Unilever Home and Personal Care in product research. After he receives his Master of Science degree, Gregory will work as a Scientist with Unilever Home and Personal Care in Trumbull, Connecticut.

ACKNOWLEDGMENTS

There are many people who I would like thank who have helped me with this work. A deep gratitude goes to the Nonwoven Cooperative Research Center for funding my research. Dr Pourdeyhimi, Chair of my committee has provided unsurpassed advice, mentorship and guidance throughout my graduate studies. His dedication to research and education was greatly appreciated. Dr. Oxenham has also been a great mentor in both my undergraduate and graduate work at North Carolina State University, who also served on my committee. Drs. Osborne and Gumpertz have provided considerable help with the statistical aspects of the research including design and analysis. Olin Stewart and Amy Minton have provided an unbelievable amount of technical advice and guidance in terms of testing. Dr William Bessey, from SpaceNet has also provided technical skill, machinery and advice throughout this work. I would also like to thank PGI, SpaceNet, BBA and DuPont for materials used in this study. In addition I would like to thank the entire staff of the NCRC for their unwavering support and friendship. Last I want to send a special thanks to my mother Amelia Grissett, father, James Phillip Grissett and my brother Kevin Grissett for their strong support throughout my education here at North Carolina State University. I could not have done this without their love and support.

TABLE OF CONTENTS

LIST OF FIGURES

LIST OF TABLES

1. Introduction

When discussing molding or thermoforming three-dimensional structures from nonwovens (or any textile), a problem arises regarding its classification. This classification has been addressed by posing several questions aimed at describing the difficulties involved in product differentiation, i.e. how thick does the substrate have to be, does embossing result in a molded or formed product, how thick does the structure have to be to be considered 3D [23]?

Representative of this classifying difficulty, the patent literature is replete with many references to formed, molded three dimensional products from nonwoven and traditional textile materials. Clarifying the classifying dilemma regarding this report, the investigations outlined in the current thesis is aimed at structures that have complex or major contours and curves. Specifically the materials produced in the study are deep-draw materials. In this context, the formed structures will have projections and depressions rising from similar *substrate* plane as displayed in Figure 1.1.

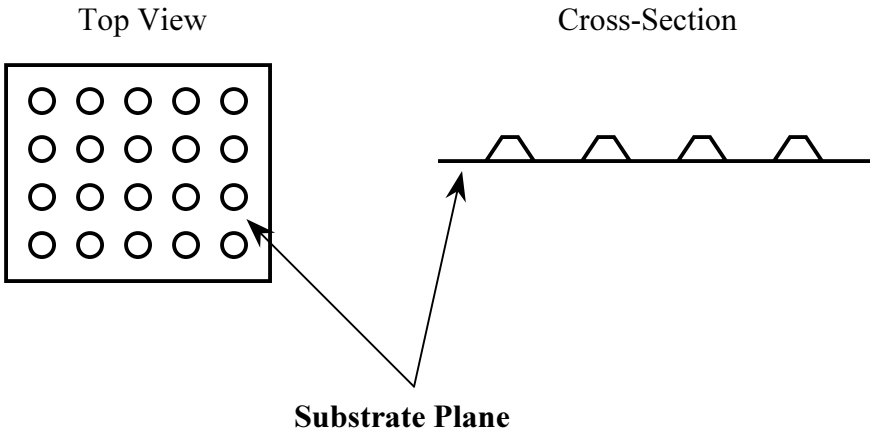

Figure 1.1 Example 3D structure produced for this study

An appropriated indication to the degree to which these projections arise from the substrate plane is the molded thickness (hereafter referred to as product thickness) to substrate thickness ratio, in this work this ratio has been measured to be between 10:1 and 20:1. Much work has been completed regarding three-dimensional textiles with the primary thrust of research, both experimental and theoretical, aimed at composite applications. The use of thermoforming to produce three-dimensional structures from woven and knitted textiles has also been thoroughly investigated. There is however a lack of information regarding thermoforming commercially available nonwoven structures into deep-draw materials. Relevant information in this regard includes: how nonwovens behave during thermoforming from a structural standpoint, the implication of processing parameters on final product properties and potential applications for three-dimensional structures from nonwovens. Therefore the current thesis investigates the production of three-dimensional deep-draw structures from nonwoven substrates via the patented SpaceNet® thermoforming system.

Unique to the SpaceNet system is ability to produce deep-draw structures with out considerable damage to mechanical characteristics. Deep-draw materials can be defined as materials that undergo large increases in surface area to achieve final form. (In this work draw ratio range from 1.25 to 2.0) This implies a more mechanical rather than a rheological phenomenon occurs with the SpaceNet thermoforming system. Conventional compression molding utilizes thermal energy to melt thermoplastic materials and then imparts pressure to reshape thermoplastics into final product from. The SpaceNet system applies thermal energy to allow adequate fiber strains to be realized that achieve the increased surface area common to deep-draw materials.

1.2 Objectives

Several objectives are proposed for this thesis. The first of which is to specifically determine what types of nonwovens *favor* thermoforming particular to the SpaceNet® system. Within in this context, moldability of webs is to be assessed based on available mold geometries. Secondly, another goal of this work is to determine how substrate deformation is influenced by relevant processing factors. Emphasis in this regard will be placed on the maximum deformation achieved during thermoforming. In addition, it is an objective to determine the effect of mold geometry on the compressive properties of three-dimensional nonwovens structures and how compressive properties vary from substrate to substrate.

2. Literature Review

The present review will briefly discuss thermoforming, three-dimensional textiles, the patent literature related to three-dimensional *nonwovens* and provides a concise review of the issues regarding forming or molding textile materials

2.1 Thermoforming

Molding in relation to polymer processing, is the shaping of thermoplastic or thermoset polymeric materials under a given heat and pressure to a required shape. Generalizing this polymer processing technique, three fundamentals steps are needed: raw material development, deformation to required specifications, and solidification after processing. Under this umbrella three types of molding operations exist: *continuous manufacture* of a product with uniform cross-section i.e. extrusion, *shaping of deformable preforms* i.e. thermoforming, *filling of a mold cavity of the desired final product dimensions* i.e. injection molding [51, 52, 53]. This study is concerned with the

deformation of pre-manufactured substrates (preforms); hence this review will focus on different types of deformation mechanisms used in regards to thermoforming.

Thermoforming is the shaping of planar thermoplastics at increased temperatures into molded articles [25] via mechanical or pneumatic means. Thermoplastic materials, by definition are polymers that can be heated, shaped and cooled repeatedly without substantial change to inherent polymer characteristics. Unique morphological characteristics allow this "thermoplastic" phenomenon to occur. Within this morphological framework, crystalline and amorphous regions describe and constitute the morphology of a polymer. Thermoforming, in the context of this thesis, is accomplished by heating the polymeric material above the glass transition (Tg) and below the melting temperature (Tm) in the presence of a nearly uniform force.

The processing of a thermoplastic polymer above its glass transition temperature transforms the polymer from a solid, glassy state to more viscous rubbery state. This transition can be envisioned as molecular movement within the amorphous regions of a polymer due the presence of thermal energy. Thermoforming processing conditions must account for stress-strain behavior of the polymer in its rubbery state. As the isothermal temperature increases above Tg, amorphous polymers become increasingly ductile (decrease in modulus are reported). For more crystalline polymers, a more aggressive temperature protocol is required to achieve similar changes in modulus [52].

Figure 2.1 displays a typical thermoforming operation. While this figure is a generalization it displays the basic components of thermoforming operations including substrate feed, mold and heating devices (here molding and heating is a simultaneous operation), cooling, and product delivery.

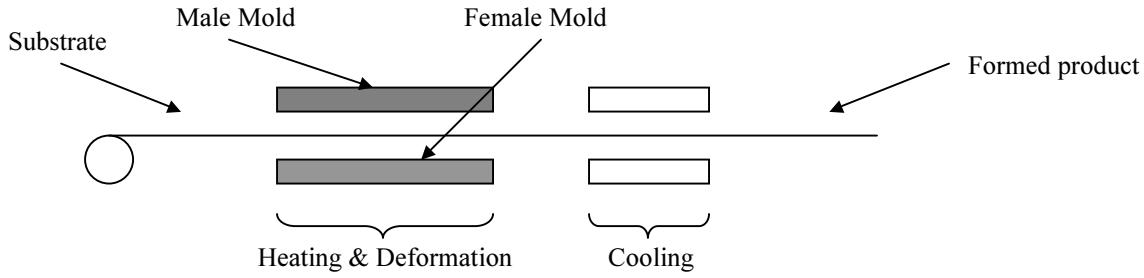

Figure 2.1 A Typical Thermoforming Operation

There are several types of thermoforming systems that can be generally isolated into three categories:

1. One-Step Forming
2. Multiple Step Forming
3. Other Variations

There are five types of one-step forming operations: drape, vacuum, pressure, free blowing and match die molding. One-step systems generally produce simple shapes with relatively short cycle times. The SpaceNet® thermoforming system would be categorized as a match-die molding system (similar to thermoforming operation displayed in Figure 2.1). Multiple-step systems are used when molded products are more complex and uniformity is important. Within these systems a *pre-stretched* substrate to pressed to a mold surface. Pneumatic thermoforming is a type of multiple –step system that utilizes a vacuum (suction) to conform a substrate to a mold surface; a second mold is also used above the vacuumed substrate to accommodate deformation. Pneumatic deformation in addition to the presence of pressure molds to accommodate deformation provides uniform wall thickness and deep draw ratios (this process is often used to make cups). [1, 3]

Pneumatic thermoforming processes are convenient for homogeneous substrates such as thin films, or plastic sheets. However, textile substrates such as woven, knit and in particular nonwovens, owing to their fiber architecture in some cases are very porous media. Void or pore size and distribution may limit the ability of a pressure differential to be achieved and substrate conformability to molds will be compromised. It would be appropriate here to utilize heated male and female molds to achieve appropriate deformation for textile substrates, such as the case for the SpaceNet System.

2.1 Three-Dimensional Structures in Textiles

2.1.1 Composites

Three-dimensional textiles can achieve their three-dimensional form *during* fabric formation or *post* processing. One method utilizes composites manufacture from continuous filaments and the subsequent formation of laminate structures (where the third dimension is achieved by the layering of separate and distinct lamina). Disadvantages to laminate composites arise from their propensity to delaminate under low stress. Another form of a three-dimensional textile structure is where the three distinct axes are achieved *during* fabric formation. In this regard, fibers (or yarns) are intertwined in a lengthwise (warp), crosswise (weft) and through thickness directions. Advantages here included the absence of distinct lamina and consequently improved delamination strength. Orthogonal weaves, three-dimensional knitted structures, and braids all fall within this category. Another form of three-dimensional textiles involves the shaping of pre-fabricated two-dimensional structures into a specific composite geometry. The resultant shapes attainable are varied, complex and limited only by the mechanical properties of the two-dimensional structures and specific formation process employed.

Composites in the form of braids, laminates of planar structures and 3D orthogonal weaves are examples of three-dimensional textile structures that find a wide variety of end-uses from transportation to construction applications. Three-dimensional braids are often used for structural applications in addition to three-dimensional or orthogonal weaves. Structural stability and design flexibility allow 3D weaves and braided composites to be commercially viable endeavors. [8,46,59]

Research into three-dimensional composite structures has comprised two major areas: mechanical property analysis of three-dimensional composite structures and analysis of the formation of three-dimensional composite structures. This review will focus on the analysis of three-dimensional composite formation.

2.1.2 Random Fiber Assemblies (Nonwovens)

Other forms of three-dimensional textiles are can be found within the nonwovens industry. Specifically, and are often molded to achieve three-dimensional form. Unique to needled felts, structural changes caused by fiber mobility within the felt allow shrinkage and elongation of the fabric in selected areas, which permits the deformation required to produce complex structures. Needle felts in three-dimensional form are a type of substrate that acquires its dimension or shape after fabric/web formation is complete (i.e. is an added process) via a molding or thermoforming process.

Air-laid technologies also exists that utilized air streams to blow or lay fibers on screens or molds thus providing a three dimensional form *during* fabric/web formation. Meltblowing has similar capabilities. Molten polymer is extruded between two high velocity laminar sheets of air and fiber is collected on a drum. Velu *et al* have initiated preliminary work utilizing meltblowing technology to produced shaped protective

garments [56]. A large market for molded textile structures, specifically molded nonwovens are in automotive applications, i.e. floorboards, headliners, acoustic insulation, fuel filters etc [28].

2.1.3 Network Materials

The patent literature also describes network materials that utilized monofilament knits and woven fabrics with subsequent thermoforming to achieve final three-dimensional form. Disselbeck *et al*. describes a three-dimensional shaped textile material via molding. The process described utilizes a highly–extensible textile sheet which is impregnated with a resin. Subsequent processing includes the thermoforming of the substrates to produce a grid-domed structure, and cure the resin. Product properties include permeability and stiffness [15, 16]. In another variant, Bessey *et al* describe a fiber network structure molded from monofilament woven and knitted fabrics with-out the use of matrix materials to impart dimensional stability. Upon molding, monofilament crossover points are not fused; the resultant structure is extremely resilient when a compressive force is applied [7, 26]. The thermoforming systems used in the previously described products is very similar to the systems used in this thesis. However, fiber networks comprised of nonwoven materials have not been completed. This has provided the impetus for the current work.

It should be noted that Huntoon, *et al* also describes three-dimensional nonwoven structure. Bi-component fibers were incorporated into a nonwoven webs with the resultant structure subsequently thermoformed to a produce a three-dimensional shape. The extent or degree of three-dimensionality and the specific process used to achieve the structures described in this patent are not consistent with materials produced for the

current work. The low-melting temperature component of the fibers used allows for moldability while the high melt temperature fiber imparts structural stability [24, 26, 49].

Common to many of the before mentioned processes, specifically for composite applications, the dimensional satiability of the formed product is often attributed to the presence of an additional constituent imparted during molding. These constituents are often in the form or resins, binder fibers or powders deposited prior to molding. The presence of heat energy during molding activates the adhesive system with the sole purpose of fiber interlocking. Because the adhesives are activated in an extended or "molded" form, once solidified, the structure retains its deformed shape. This has been a primary method for manufacturing three-dimensional products for textile substrates and is analogous to thermal bonding of nonwoven webs (when binder fibers or powders are used for web bonding) [65].

2.2 Forming Studies

Determining an appropriate balance between mechanical deformation and rheological melt is critical to achieve maximum deformation without degradation. Characterizing the deformation of the substrate induced by thermoforming becomes important to minimize redundant and costly trials from a developmental point of view.

Traditional forming techniques used in the metal industry attempt to characterize the formability of the substrates before processing is conducted. With the growth of composites use in automotive, marine and industrial settings, these analytical tools have been extrapolated to evaluate the formability of various substrates including textile preforms. Various analytic tools that have been developed for textile-related substrates will be reviewed included mapping analysis, formability studies, forming limit diagrams,

and strain field analysis. It is an objective of this review to evaluate if formability studies could and should be used on various nonwoven structures as a criterion for thermoforming.

2.2.1 Composite Sheet Forming

As described previously, various processing methods are available to achieve structures that can be defined as three-dimensional in final form. A procedure for modeling the *formation* of final products proves useful from a developmental standpoint. Composite sheet forming closely resembles the processing techniques used in regards to the current thesis. Therefore issues that arise in formation analysis or modeling of composite sheet forming can be insightful when evaluating the formation of three-dimensional structures from nonwovens. Two major approaches have been used historically for composite sheet forming modeling: mapping and mechanics based methodologies. The earliest and most simplistic analysis tools involve mapping approaches. Comparatively, mechanics based approaches utilized constitutive equations to predict product properties and shape over the course of forming and is therefore a more difficult approach.

When utilizing modeling techniques several assumptions are made. First it is assumed that the material is *incompressible* and second, it is assumed that the material is *inextensible* in the fiber direction. Thus, for unidirectional structures, deformation is achieved via shearing along the fiber direction. For wovens fabrics, trellis shearing accounts for changes in product dimension. (It should be noted the yarn intersections act as pivots with free rotation but no slippage). For knitted structures deformation is achieved via yarn straightening, trellis shearing and yarn slippage [34].

2.2.1 Formability

Thermoforming of nonwoven substrates is accomplished through a combination of two material phenomena: rheological and mechanical deformation. Rheological deformation implies that a certain amount a molecular movement is induced though the application of heat to the substrate thus softening the fiber to the point of laminar movement. To maintain fibrous characteristics without considerable change to molecular orientation and crystallinity, a forming temperature above the glass transition and below the melting temperature is used. Mechanical deformation is concerned with the mechanical behaviors of the substrates on a macro scale. In conventional thermoforming processes where deep draws are introduced into the substrate, four fundamental modes of mechanical deformation are observed as seen in Figure 2.2: in plane tension, transverse compression, in-plane shear and out-of-plane bending [44, 61,62,63]. While these are general deformation modes, complexity in mechanical deformation will vary with more geometrically complex molds.

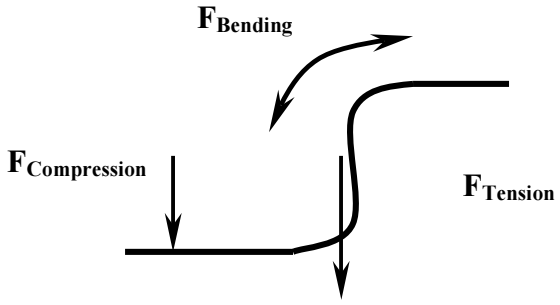

Figure 2.2 Mechanical Deformations in Thermoforming A Dome Structure [41,61]

Formability therefore becomes a dichotomous issue. In the context of mechanical deformation, formability evaluation is concerned with the four types of deformation

mechanisms mentioned previously that are present during the thermoforming process. Yu et al, studied the correlation between the four fundamental modes of deformation (tensile, bending, in-plane shear, and out-of-plane bending) with a derived conformability index, C.I. The CI was obtained from the measured forming energy of various woven preforms.

$$CI = \frac{1}{U} \qquad (1)$$

CI = Conformability Index
U = Forming Energy, energy required to deform the specimen to a preset displacement

Utilized in this study, was a hemispherical plunger attached to a modified Instron crosshead. The load required to deform a sample to a predetermined depth was recorded, and the area under the load displacement curve produced the forming energy required to deform the specimen. This method is very similar to the Mullen bursts test except that the plunger used is metal, in lieu of a rubber ball with increased pressures aimed to achieve failure.

In terms of rheological properties, appropriate heat and pressure used during the thermoforming process, in conjunction with relative time spent in the mold, and affects the dimensional stability of formed products. This study (Yu *et al*.), due to the use of graphite preforms did not attempt to evaluate the rheological aspects of formability. Optimizing temperature-pressure-time combinations in addition to selecting appropriate substrates in terms of mechanical behaviors will allow maximum deformation without degradation when manufacturing three-dimensional fiber networks. In addition, utilizing various molds will change the forming energy values and the type of mechanical deformation that is prevalent in that particular forming process [44,61].

2.3.2 Forming Limit Diagrams

As described previously, many of the analytical tools used to evaluate the formability of sheet metal have been extrapolated and used to access the formability of thermoplastic composites. Dessenberger *et al.* utilized forming limit diagrams to access the formability of random fiber mats and developed a mathematical method to express this formability in quantitative manner. The basis for forming limit diagrams was to limit substrate failure during processing, these failures as classified by Dessenberger *et al*. including wrinkling or tearing during thermoforming and variations in the amount of stretch induced by forming from one area of the substrate to another. Within composites processing, variants in stretch lead to variations in pore size, which in turn lead to permeability differences effecting resin distribution [14]

The experimental method was aimed at how to apply controlled biaxial strains, defining failure in random fiber mats, and how to convey these results in mathematical form. Assumptions made in this analysis are that the sheet is loaded in-plane stress during forming and the sheet is completely isotropic. Given this, Dessenberger cites that the deformation at any point is characterized by strain components $\varepsilon 1$ and $\varepsilon 2$ in the principle strain directions, or by stretch ratios defined as $\lambda 1$ and $\lambda 2$. The forming limit diagram is essentially a map in $\lambda 1$ - $\lambda 2$ space. Within this space, limits or boundarys are set based on various mechanical tests (uniaxial tensile, shear, biaxial stretching) to failure. As limits have been set, an ideal forming situation would produce strains that fall within the limits established during testing [14]. In addition, a formability function

was developed that describes the local deformation in the mat relative to the allowable deformation.

Drawbacks regarding this method lie firstly in the assumptions regarding the properties of random fiber mats or nonwovens. It is well known that many nonwoven structures can display highly anisotropic behavior, due to fiber orientation, and that this anisotropy is not often "negligible." In addition, the type of deformation mechanisms present in thermoforming can be very complex, i.e. the loads experienced by the substrate may not be in-plane.

2.3.3 Drawabilty

The largest possible draw ratio or limiting draw ratio obtained before failure classifies drawabilty. Draw ratio in conventional uses encompass the use of area or diameter ratios for before and after molding operations. As the previous techniques were used for sheet metal forming analysis, such was drawabilty determination used to access the formability of self-reinforced thermoplastic sheets [44]. Relative to this study on deep drawing, in terms of nonwoven forming, the draw ratio could be defined the surface area of the formed part to the surface area of the substrate. Specifically, the surface area at which failure occurs could be sued to determined the limiting draw ratio of the substrate.

$$LDR = \frac{SA_A}{SA_B} \qquad (2)$$

SA_A = Surface area after molding
SA_B = Surface area before molding

Pede *et al* postulated that formability of sheet-like materials is determined in great deal by mechanical properties of the material. Specifically, he proposed similar

deformation mechanisms in forming a small cup to the deformation mechanisms proposed by Yu *et al.* Often, yield strength, tensile strength, total elongation, and yield point elongation are measured and related to drawing, but do not commonly have a direct or unknown relation to drawability.

Specifically, Pede *et al* experimented on the drawability of self-reinforced thermoplastic sheets regarding the formation of a simple cup. Pede *et al* states that increasing the load resistance of a material in the thickness direction relative to its load resistance in the plane of the sheet will improve the drawability of materials. In this regard anisotropic materials have improved drawability over isotopic materials. Additionally, anisotropy is often described as two-dimensional phenomena displayed by apparent differences in the planar properties of the sheet. However, normal anisotropy could be more pronounced than planar anisotropy a determining factor as related to drawability [44].

2.4 Nonwovens and Thermoforming

Specific to this study, nonwoven fabric deformation depends primarily on inherent fiber properties, fiber orientation and the degree of bonding/entanglement. Nonwoven fabrics often display anisotropic behavior with variations in properties across the width and length of the web. However, mechanical properties of nonwoven webs follow fiber architecture with a great reliability. It is also observed that the machine direction for certain types of webs will carry the majority of the orientation of fibers. It is this variance in orientation that caused shift in properties to occur when measuring properties between the MD and CD (or anisotropy).

Despite the types of deformation found in the thermoforming processes described previously, elongation is a parameter of importance due to its relationship to tensile, shear, and to some extent bending properties of the web. Thermoforming a substrate into a complex structure with projections and deep draws rising from an initial plane is a process that increases the total surface area of the substrate. Given the substrate is of finite area, local deformation allows this increase in surface area to be achieved and the three-dimensional fiber network to be realized. Local deformation can be attributed to the extensibility of the substrates under thermoforming conditions, while the tensile, bending, and compressive proprieties of the web limit failure.

This formability failure may display different mechanical properties than formed products that do not "fail." It is assumed here that the dimensional stability of formed products is related to the amount of mechanical and thermal degradation present, if any, incurred during thermoforming.

3. SpaceNet Thermoforming Process

The SpaceNet® formed fiber system is method for producing three-dimensional structures from nonwoven substrates is. Unique to this system is that a thermo-mechanical deformation is utilized to produce three-dimensional structures without the use of an adhesive system during product formation (although one can use a binder). Patents Nos. 6,007,898 and 5,851,930 describe this process, which was primarily aimed at using traditional textile materials such as woven or knitted fabrics manufactured via monofilaments. The current work extends the previous work to include nonwoven substrates.

A 50-Ton hydraulic press was utilized for initial molding trials and is displayed schematically in Figure 1.2. Important processing parameters include the following:

1. Operating Temperature (T_O)
2. Residence Time (R_t)
3. Mold Time (M_t)
4. Stop Height (S_t)

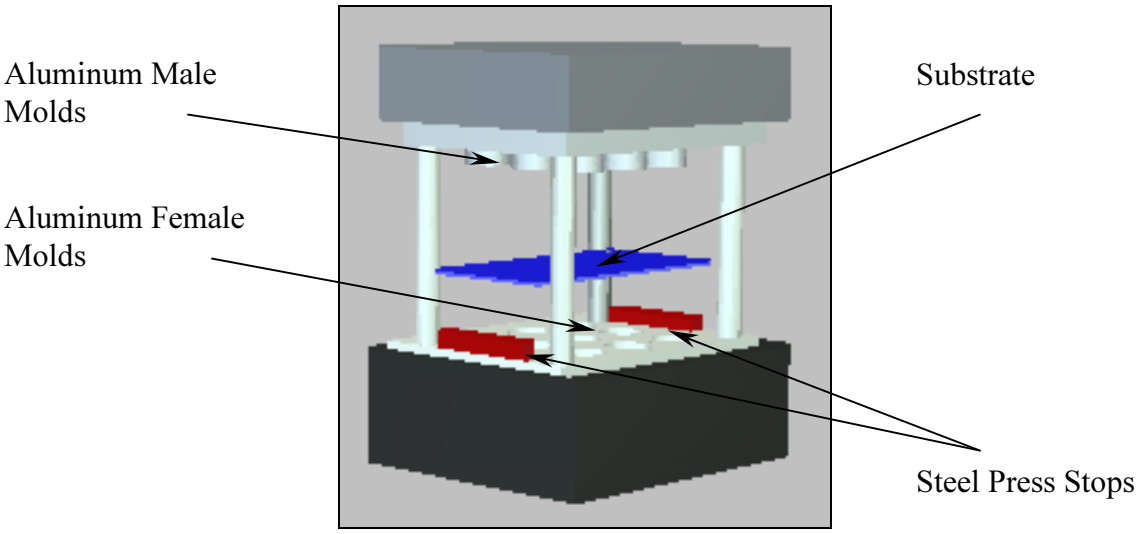

Figure 3.1 SpaceNet Hydraulic Press

3.1 Operating Temperature

Operating temperature is the temperature at which substrate molding will occur. Through the application of heat, molecular movement is induced within the polymer thus softening the fiber. This fiber softening allows deformation to occur at lower stress levels compared to the stress levels required to deform the fiber when processed at ambient temperatures (15˚ - 30˚ C). To maintain fibrous characteristics without considerable change to molecular orientation and crystallinity, a forming temperature (operating temperature) above but closer to glass transition and below the melting temperature is used. Table 3.1 displays common operating temperatures for the polymers used in this study.

Table 3.1 Operating Temperatures by Fiber Type

Fiber	(^{o}C)
PP	110-120
PET	190-205

Selection for operating temperature was based primarily on the past processing trials for each fiber type used.

3.2 Residence and Molding Times

Residence time is defined as the time permitted for *substrate preheating* to occur in this molding process. Residence time should be sufficient to induce and allow for the molecular movement and the subsequent fiber softening described previously. Refer to Table 3.2 for residence times used for each fiber type used in this study.

Table 3.2 Residence Time by Fiber Type

Fiber	Residence Time (s)
PP	30-90
PET	30-60

Because a direct preheating chamber is not available, machine design dictated preheating the substrate by lowering the press to the point where the heated male and female molds are in direct contact with the substrate. The time that the press is in the lowered position before deformation occurs is recorded as residence time (in seconds) (refer to figure 1.3). We assume that the heated molds resting on the surface of the substrate would allow for adequate thermal transfer and induce fiber softening. After preheating is complete (as defined by residence time) the press is completely lowered to

induce substrate deformation. Mold time is therefore measured as the time the substrate is in the deformed state, refer to figure 1.4 for schematic representation. It is important to note that mold time should be sufficient to set the substrate into its deformed state. Insufficient mold times will produce products that will not retain their respective shapes (or three dimensional effect).

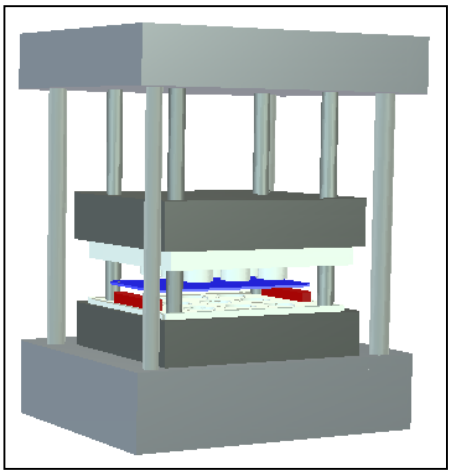

Figure 3.2 Press in Residence Phase

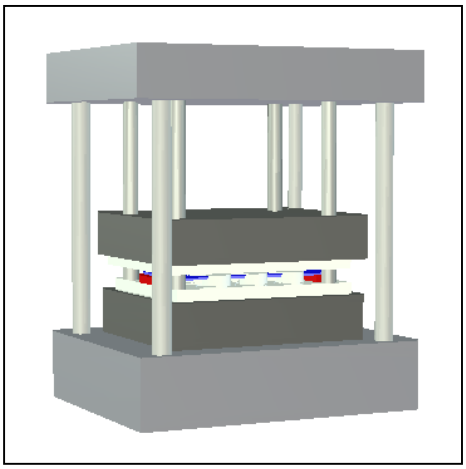

Figure 3.3 Press in Molding Phase

As with operating temperature, residence time and mold time were initially selected based on previous trials for similar fiber types and held constant for comparative

purposes for the initial trial. Table 1.3 displays the mold times for each fiber type used in this study.

Table 3.3 Mold Time by Fiber Type

Fiber	Mold Time (s)
PP	30-60
PET	15-75

3.3 Stop Height

Stop height is defined as the measured height (mm) of the steel press stops used during thermoforming. Steel press stops limit the depth of penetration through the substrate achieved by the male mold. Stop height therefore impacts formed product dimensions, specifically dome height, which is a measure of formed product thickness. Stop heights are interchangeable and can be varied to achieve the required deformation for each substrate used in this study. Smaller stop heights allow the male mold to penetrate the female mold to a greater depth; this in turn produces thicker projections on the substrate. Comparatively, large stop heights limit the depth achieved by the male mold, which in turn produces smaller projections rising from substrate plane.

3.4 Mold Geometry

Two types of mold geometry configurations are available on the SpaceNet system. The first is a male-female mold configuration and produces grid-domed structures similar to the structure shown in figure 1.1. The dimensions of the male-female mold combinations can be varied to produce different structural dimensions in the final product. Notably, the male pin and female holes do not intimately match or touch during molding. For example a ¼" male pin diameter is often used with a 3/8" female hole diameter.

The second type of mold geometry available on this thermoforming system is defined as "interdigitated." This system utilizes two male molds of similar dimension offset (refer to figure 1.4). The type of structure produced using the "interdigitated" system is comprised of projections and depressions rising/falling from the substrate plane as defined previously. Both male molds used in this configuration have equal pin diameters. Three pin diameters are currently available: ½", 3/8" and ¼".

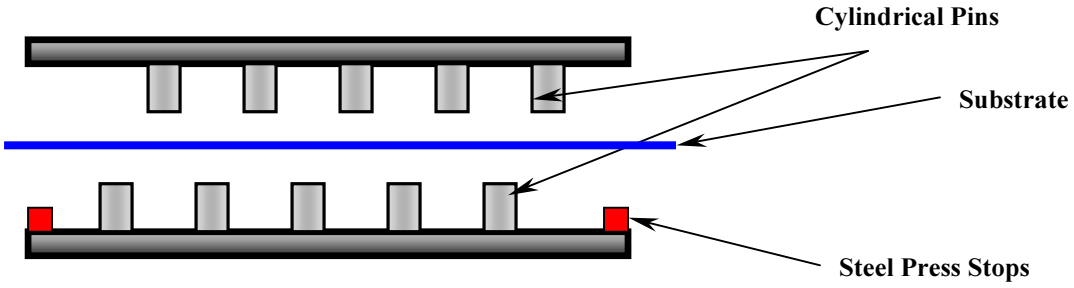

Figure 3.4 Interdigitated Mold

Experimental work will be divided into three areas: moldability and compressive properties of nonwoven substrates, evaluating of the maximum deformation achieved and evaluating the effect of mold geometry on compressive properties. With assessing the moldability of webs, the ODF will be assessed and its relation to substrate deformation during molding will be described and related to success or failure in molding. In addition, structural parameters such as the use of short staple systems or filament-based systems will also be used to assess moldability. Evaluating the maximum deformation achieved will involve measuring the effect of temperature, residence and mold time on the maximum dome height or thickness attained. The last component of this work will vary the mold geometry and map how compressive properties shifts with changes in mold geometry by web/substrate.

Additionally, the SpaceNet thermoforming system is unique process compared to other types thermoforming/molding operations. In particular the deep-draw characteristics of the materials produce via this system is the critical difference compared to systems that produce textile materials with a substantial third dimension. As with other types of thermoforming systems, in particular fiber manufacture, draw-ratios are used to assess the amount of deformation imparted during product manufacture. Draw-Ratio (DR) in the context of this report is defined via the following relation:

$$DR = \frac{A_{SF}}{A_I}, \qquad (3)$$

Where A_{SF} is the total *final surface area* created via thermoforming from an initial surface area, A_I. It should be noted that A_{SF} is a calculated parameter, and has only been used to quantify the draw ratio for three-dimensional structures produced from the male/female mold geometry. Three-dimensional structures produced for the current report have theoretical draw ratios ranging from 1.16 to 1.91, depending on substrates basis weigh amount of deformation imparted and specific mold geometry used. Generally the draw ratio will increase as a function of product thickness increases and pin diameter decreases (Graph 1, Appendix A.). Appendix A provides a more detailed description of draw-ratio with the methodology for calculating the final surface area used in above equation.

4. Experimental Work: Determination of Nonwoven Moldability

4.1 Substrates

Eight commercially available nonwoven substrates were obtained for this study. Six spunbond fabrics were obtained from both BBA and Dupont and two hydroentangled

fabrics acquired from PGI. The following table displays physical characteristics for the substrates obtained.

Spunbond nonwovens are manufactured via extrusion of selected polymer resins followed by collection of the filaments on a moving belt. The 'web' produced is then bonded via calendar rolls. Sample Nos. SF 27, SF 44 and SF 94 are all polypropylene and represent the same webs in terms of processing conditions. The only differentiating parameter is the basis weight, as seen in Table 3.1. Sample nos. 2295, 2033 and 2440 are comprised of polyester fibers and represent three different webs, with basis weights held constant, but varying fiber properties.

Table 4.1 Spunbond Samples

Sample	Fiber	g/m^2	Thickness (mm)	Tensile Strength (kgf) MD/CD	Strain at Break MD/CD	Fiber Cross Section	Fiber Diameter (μ)
SF 27	PP	90	.38	9.3/12.3	27/35.6	R	40-50
SF 44	PP	150	.46	23.9/26.5	39.5/41	R	40-50
SF 94	PP	320	.75	65.7/56.1	35.1/37	R	40-50
2295	PET	100	.43	10.7/9.5	62.1/64.8	R	15
2033	PET	100	.45	12.2/7.8	46.5/46.3	TRI	20
2440	PET	100	.53	5.5/4.2	42.1/48.3	TRI	20

Hydroentanglement is a mechanical bonding mechanism used to entangle fibrous webs utilizing high-pressure water jets. Web formation was accomplished via carding line utilizing short staple polyester fibers followed by subsequent hydroentangling.

Table 4.2 Hydroentangled Samples

Sample	Fiber	g/m^2	Thickness (mm)	Tensile Strength (kgf) MD/CD	Strain at Break MD/CD	Fiber Cross Section	Fiber Diameter (μ)
PGIT	PET	100	1.0	43.5/18.3	27/35.6	R	na
PGIH	PET	170	1.0	18.4/15.1	39.5/41	R	na

The following figures display the tensile properties of the substrates in terms of both peak load and strain at break.

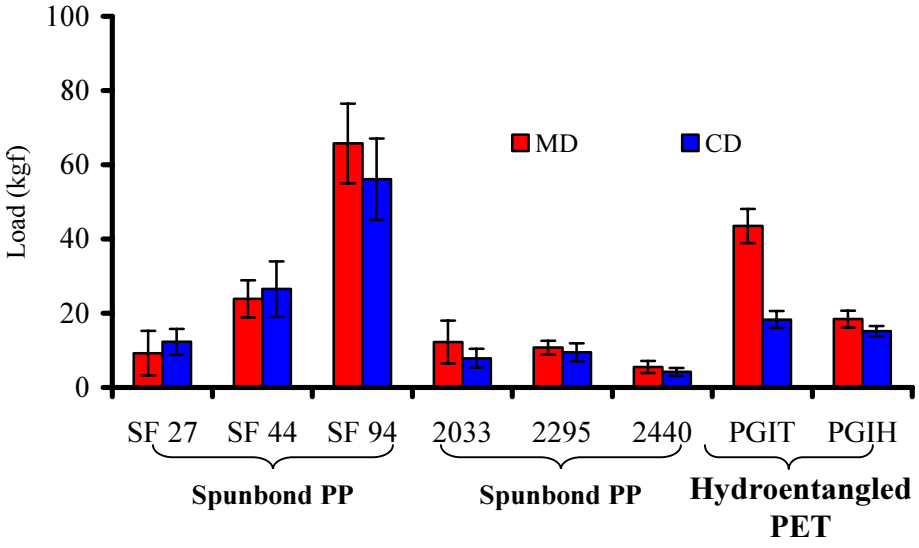

Figure 4.1 Tensile Strength

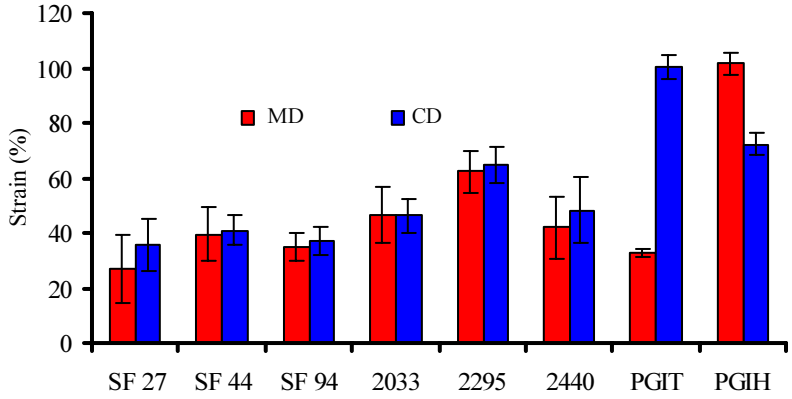

Figure 4.2 Strain at Break

Anisotropic behavior in terms of peak tensile load and test direction is a common characteristic of nonwoven mechanical properties as displayed by Figure 4.1. However, the peak strain at break was found to be more anisotropic for the *hydroentangled* substrates than for the spunbond substrates (refer to figure 4.2). Contributing to the

phenomena are the different *modes* of tensile failure found in filament-based substrates compared to short-staple based substrates.

Nonwoven fabric deformation depends primarily on inherent fiber properties, fiber orientation and the degree of bonding/entanglement. Often nonwoven fabrics display anisotropic behavior with variations in properties across the width and length of the web. However, mechanical properties of nonwoven webs follow fiber architecture with a great reliability. The following figures display the fiber orientation of our samples by fabric and polymer type, and provide a graphical representation for anisotropy.

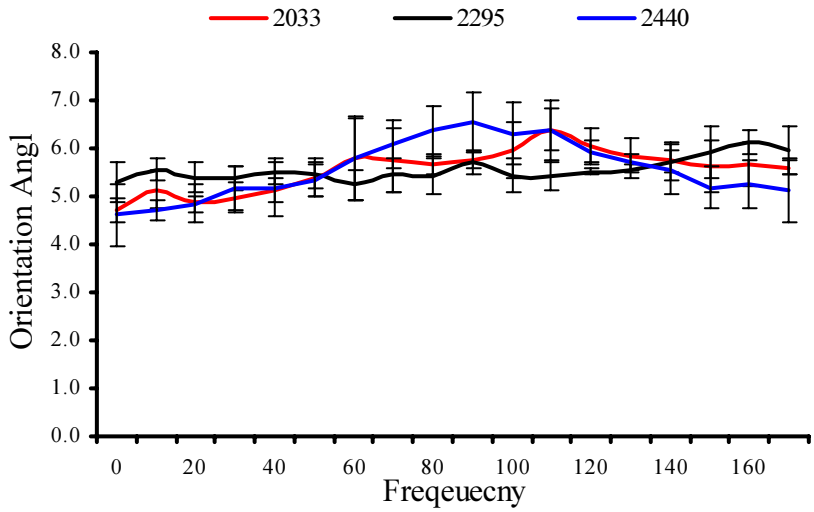

Figure 4.3 Spunbond PET Fiber Orientation Distributions

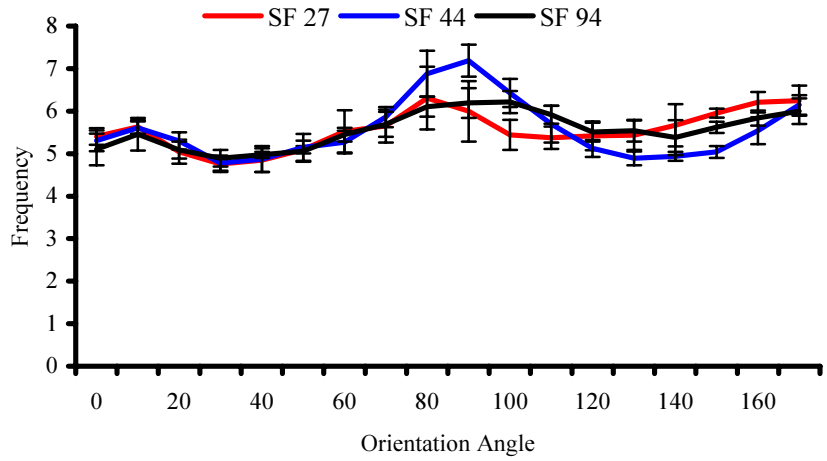

Figure 4.4 Spunbond PP Fiber Orientation Distributions

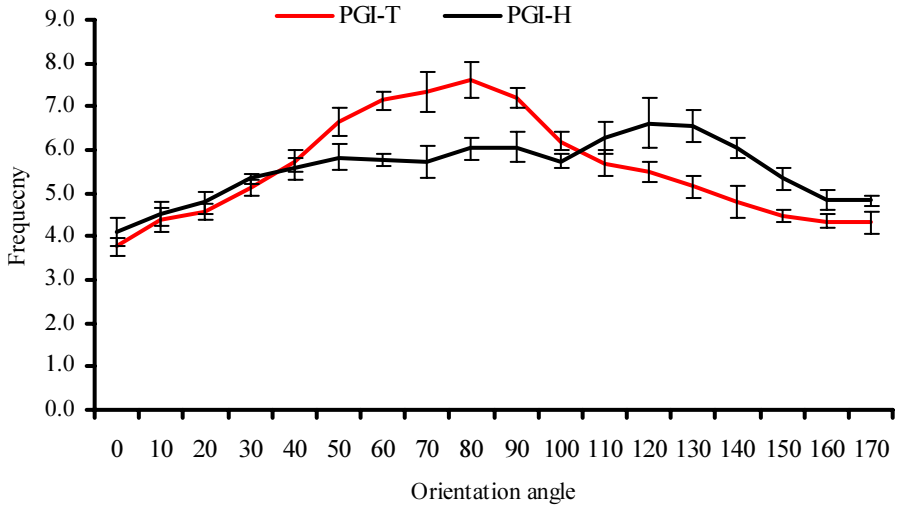

Figure 4.5 Hydroentangled PET Fiber Orientation Distributions

As described above, the ODF figures for the hydroentangled samples display a greater anisotropy than the spunbond samples. This is evidenced by the reported cosine squared anisotropy value of -.146, and -0.085 for PGI-T and PGI-H, respectively, which consequently were the *highest* cosine squared anisotropy values reported for all samples analyzed refer to table 4.3 Below.

Table 4.3 Fiber Orientation Uniformity Data

Sample	Dominate Angle	Cosine Squared Anisotropy
2033	113.056	-0.055
2295	155.317	-0.021
2440	100.075	-0.078
SF 27	135.919	-0.033
SF 44	94.348	-0.044
SF 94	112.843	-0.038
PGI-T	81.786	-0.146
PGI-H	103.395	-0.085

4.2 Formed Product Analysis

4.2.1 Failure Mechanisms

Thermoforming a substrate into a complex structure with projections and deep draws rising from an initial plane is a process that increases the total surface area of the substrate. Inherent fabrics properties will determine how the substrate surface area is increased. The property variations between the webs described above can be attributed to processing conditions, failure mechanisms (in terms of thermoforming) in similar manner may also vary with different processing conditions. In this regards, "success" in thermoforming is described as adequate deformation of the substrates *without* the presence of holes produced by the interaction of male and female molds during processing. Comparatively, a 'failure' is where holes *are present* after thermoforming.

To establish a basis for comparing 'successes' and 'failures' in substrate thermoforming, the initial formed product analysis considers products produced using similar stop heights. While operating temperatures, residence and molding times are different for varying polymer types, within polymer type and fabric type utilized constant processing parameters (refer to table 4.4).

Table 4.4 Processing Conditions –Analysis 1

Sample	Fiber	Fabric Type	g/m^2	T_O	R_t	M_t	S_t
SF 27	PP	Spunbond	90	110	60	60	**12.6**
SF 44	PP	Spunbond	150	110	60	60	**12.6**
SF 94	PP	Spunbond	320	110	60	60	**12.6**
2295	PET	Spunbond	100	190	30	30	**12.6**
2033	PET	Spunbond	100	190	30	30	**12.6**
2440	PET	Spunbond	100	190	30	30	**12.6**
PGI-T	PET	**Hydroentangled**	170	190	60	30	**12.6**
PGI-H	PET	**Hydroentangled**	100	190	60	30	**12.6**

The first molding trial produced only two failures: PGI-T and PGI-H. The following figure depicts these failures.

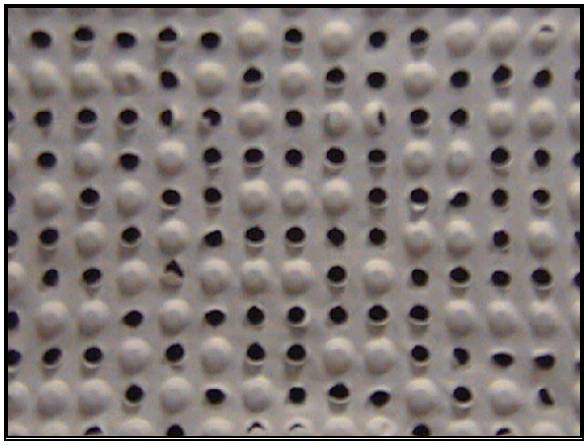

Figure 4.6. Holes produced on PGI-T and PHI-H

From this it can be seen that the hydroentangled substrates failed given all substrates were molded utilizing similar processing conditionings, most importantly stop height. Common to the hydroentangled substrates are that both are derived from short staple manufacturing systems. It is apparent that filament bases systems fail in tension in

a different *manner* than short staple systems. It is plausible that the spunbond substrates allow a greater amount of draw during thermoforming while maintaining adequate cover over the dome. Short staple systems comparatively will not allow as much fiber draw during thermoforming hence produce holes at similar stop heights to spunbond samples.

Another trend specific to the hydroentangled substrates is the considerable difference in anisotropic behavior for strain at break values compared to the other spunbonded substrates (refer to Figure 3.2). This trend is due to the anisotropic fiber orientation found for the hydroentangled samples (Figure 3.5). For the molds used in this study, a more 'uniform deformation' under a load is a favorable property (in terms of MD and CD). Utilizing a web that displays a more random distribution of fiber orientation achieves this uniform deformation and would constitute a more moldable web. The spunbond substrates used in this study display uniformity in fiber orientation, which allows uniform strain to break values to be realized. It is thus concluded the moldability can be associated with fiber architecture, more specifically, where mold geometry governs uniform deformation, a uniform distribution of fiber favors thermoforming in terms of moldability.

4.2.2 Compression-Recovery Properties

Concluding the formed product analysis is the evaluation of the compression-recovery properties of the formed products produced thus far. No 'standard' test method exits for the compressive properties of nonwoven materials. Consequently, a method was developed which gave the following parameters were use in this evaluation:

-Platen Separation:	10 mm
-Crosshead Speed:	1mm/min to 40 % strain
-Specimen thickness:	taken at .005 kgf
-Type:	CRE

-Sample Size: $10cm^2$

A 40 % strain value was selected so as to accommodate the small structural changes found in the domes. The type of deformation during substrate molding produced a truncated cone as displayed in Figure 4.7. Approaching 40% strain ensures that compression would surpass the point where the dome changes from a more cylindrical shape to a more conical shape. In doing so the effect of this shift in dome dimensions on compressive properties would be accounted for.

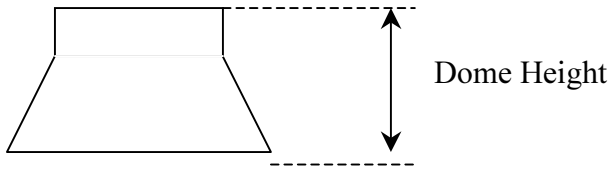

Figure 4.7 Dome Structure

The following compression–recovery curves represent alls samples produced using the processing conditions stated in table 4.3. For comparative purposes the hydroentangled substrates, process at a stop height of 14.4 mm are included here (due to failure incurred at 12.6 mm as described previously).

4.2.2.1 Spunbond Polypropylene

Observing samples SF 27, 44 and (refer to figure 4.8 and 4.11 below). These samples represent the same products at three different basis weights (refer to table 4.4 of data regarding substrate properties). An initial indication is given as how increases in basis weight affect the compressive properties of three-dimensional nonwovens.

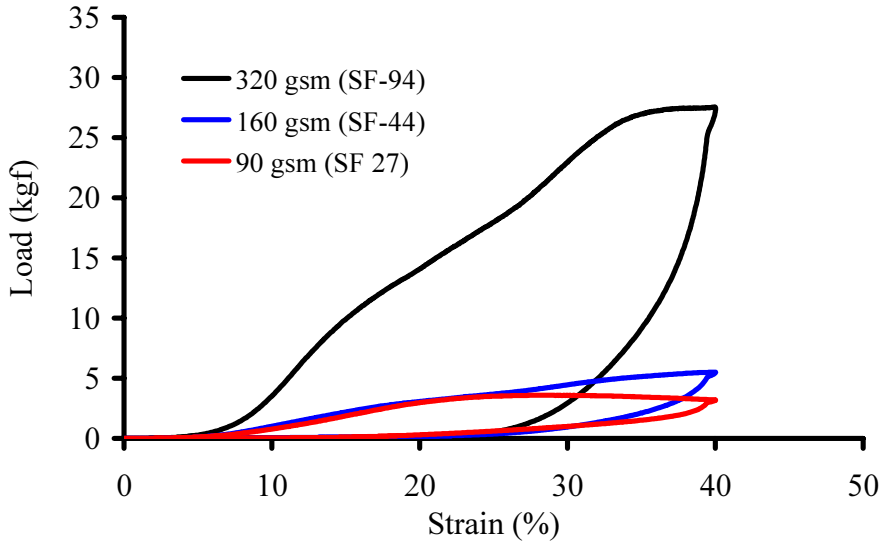

Figure 4.8 Compression Recovery for Spunbond Polypropylene

For polypropylene spunbond samples is it observed that increases in basis weight improve the compressive properties of formed products. However, lighter webs display a different compressive behavior than heavier webs. A closer look at SF 27 in figure 3.7 reveals that after a certain strain (~25%), the force required to deform the sample will decrease. Comparatively, for SF 94 (320 gsm), the force required to deform the sample continues to increases past 25% strain and then plateaus closer to 40% strain. Maximum resistance to compressive forces is achieved at lower strains for lighter webs, which is in part due to inherent stiffness of the substrate and the number of fibers per unit area available to resist compressive forces. Differences in dome geometry also play a role in this behavior and will be addressed in later.

4.2.2.2 Spunbond Polyester

Spunbond polyesters substrates had comparable basis weight values: variation between substrates is therefore attributed to different processing conditions and partly

different fiber cross sections employed in extrusion. When isolating the polyester spunbond samples, i.e. sample 2033, 2295, and 2044, incremental differences in compressive stress are observed. . Substrates 2440 and 2033 utilize trilobal cross-section while 2295 employs a circular cross section during substrate manufacture. Statistical analysis for peak load values makes this a robust conclusion. Round or circular fiber cross sections exhibit greater stiffness values for similar diameter when compared to other cross sections. Improved or increased fiber stiffness will therefore have a concurrent impact on dome properties. This may explain why sample 2295 reports a larger compressive stress than the other the samples. The compression recovery behavior of the PET samples display differences regarding at what strain values that peak loads are experienced. Figure 4.9 displays these differences.

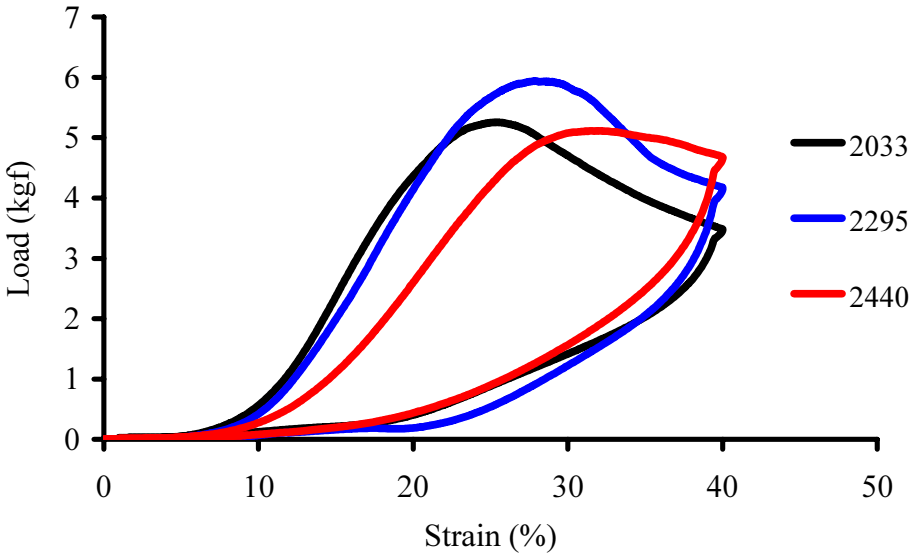

Figure 4.9 Compression Recovery for Spunbond Polyester

Variation in compressive properties could be attributed to the variation in mass *uniformity* of the web presented in the above graph. Notably, all samples experience a

drop in the compressive force required to deform the sample after certain strain values. More specifically, 2033 and 2295 encounter a more dramatic drop in compressive force required to deform the sample further (to 40%).

4.2.2.3 Hydroentangled Polyester

Because failure occurred at a stop height of 12.6 mm for the hydroentangled substrates described previously, the following compression-recovery curves (Figure 4.10) are taken from substrates processed with a stop height of 14.4 mm. The compressive – recovery behavior of hydroentangled samples tend to display greater recovery compared to other samples, in addition it is observed that peak load may not have been achieved at 40% strain. The failure to achieve peak load is contributing factor to the improved recovery of hydroentangled structures.

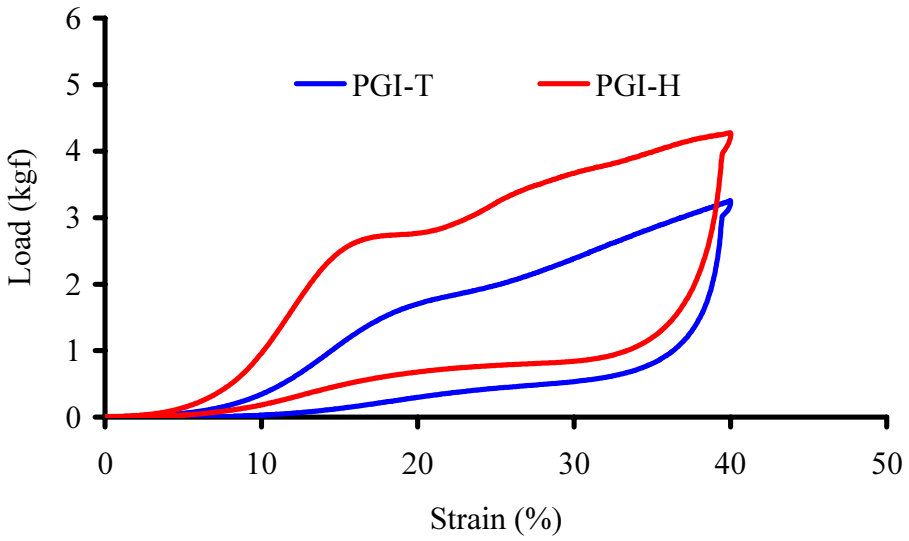

Figure 4.10 Compression Recovery For Hydroentangled Samples

4.2.2.4 Compressive Stress Comparisons for All Substrates

Figure 4.11 below displays the compressive stress values for all substrates studied. ANOVA analysis reveals that the mean compressive stress differs significantly between substrates ($p < 0.00001$) (refer to figure 4.11). .

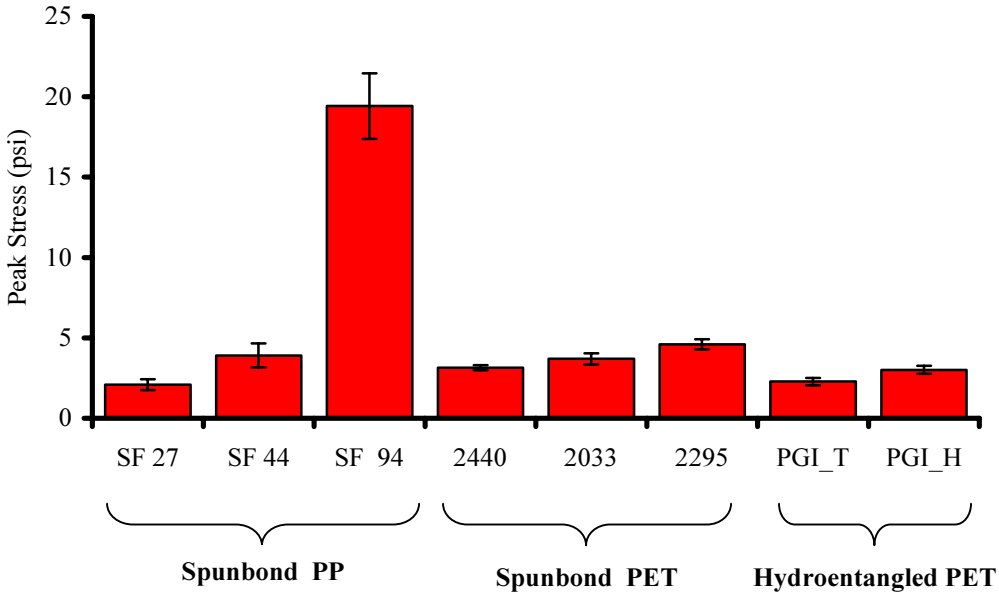

Figure 4.11 Compressive Stress: All Substrates

Table 4.5 Analysis of Variance for Differences in Compressive Stress

Source	DF	Sum of Squares	Mean Square	F Value	P-Value
Substrates	7	1401.47035	200.21005	307.922874	< 0.00001
Error	40	26.0078178	0.65019544		
Total	47	1427.47817			

The compressive secant modulus (to 15% strain) was also measured for all substrates. Modulus to 15-% strain was selected based on observation that up to 15% strain, the *rate of loading* has increased significantly from O-% strain for all substrates evaluated. Secant modulus to 15-% strain becomes a material property only useful in comparing one sample to another within the confines of this study. Referring to figure

4.12 it is observed that the modulus means differ significantly among substrates ($p < 0.001$).

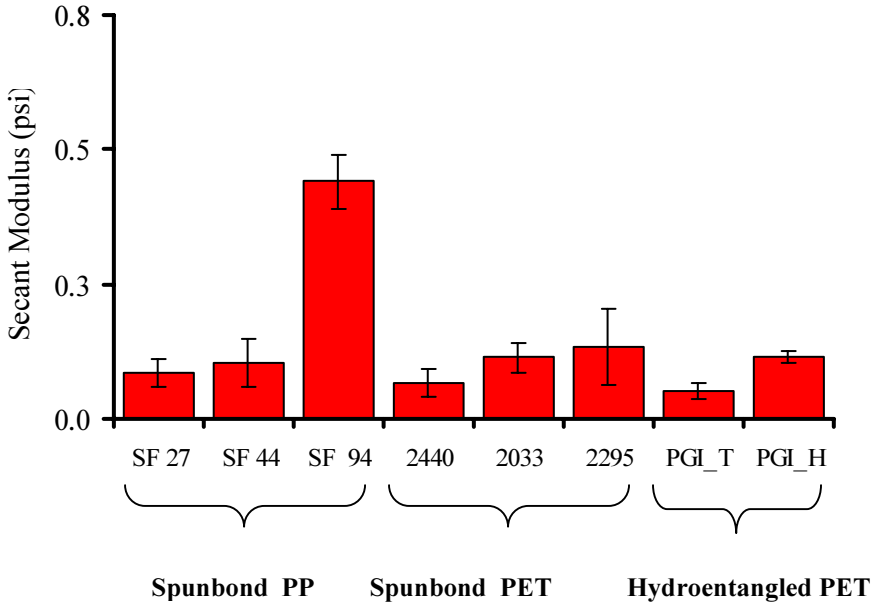

Figure 4.12 Compressive Secant Modulus: All Substrates

Table 4.6 Analysis of Variance For Differences in Compressive Secant Modulus

Source	DF	Sum of Squares	Mean Square	F-Value	P-Value
Substrate	7	0.653	0.09327	61.6592	< 0.0001
Error	40	0.061	0.00151		
Total	47	0.713			

Grouping samples by basis weight, variation does appear based on polymer type. For example, SF 27, 2295, 2033, 2440 and PGI-H all report basis weight values around 100 g/m^2. Sample SF 27 is comprised of polypropylene and reported the lowest compressive stress across spunbond and hydroentangled samples at similar basis weights. Within polypropylene samples (SF 27, SF 44, and SF94), increases in basis weight are associated with increases in compressive stress. It is hypothesized that the "level of bonding" within nonwoven web plays a fundamental role in determining the compressive

properties of nonwoven substrates. Measuring the flexural and tear properties for a given substrate may *indicate* the "level of bonding" imparted during substrate manufacture.

Figures 4.12 and 4.13 displays the trapezoidal tear strength and bending stiffness, respectively for each substrate. Trapezoidal tear strength via ASTM-D5733-99 was used to assess tear properties [71]. Because the substrates are relatively stiff materials the cantilever-bending test proved inadequate. Therefore, flexural strength was measured via four-point bending utilizing two loading noses that impact *and bend* a substrate sample that rests upon two supporting noses [3]. A load–extension curve is therefore produced. For elastic materials catastrophic failure does not occur, therefore *peak* load was used as a measure of flexural strength when bending a given sample. Machine direction (MD) samples were tested with loading noses flexing a sample perpendicular to the machine direction while cross direction (CD) samples were tested with loading noses flexing a sample perpendicular to the cross direction.

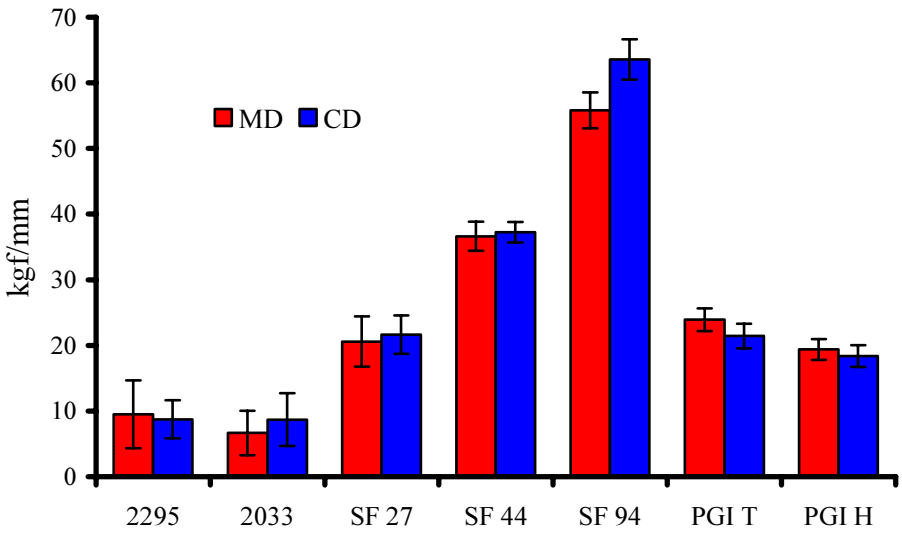

Figure 4.13 Trapezoidal Tear Strength

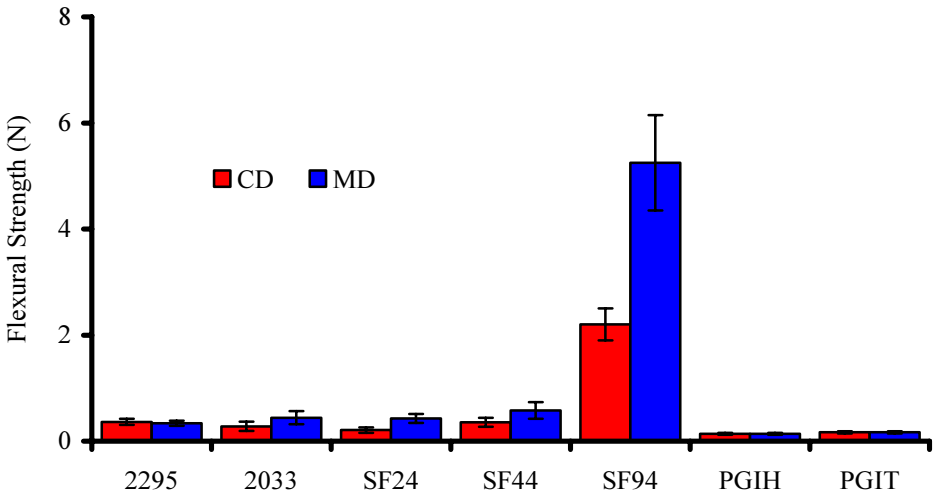

Figure 4.14 Substrate Flexural Strength

It was hypothesized the compressive stress is associated with several substrate characteristics including basis weight and the "level of bonding". The compressive stress of all formed products (y, or dependent variable) was regressed against independent variables: substrate tear strength (x_1), flexural strength (x_2), and basis weight. (x_3). Note that one replicate was used thus providing the following (full) linear model:

$$Y_i = \beta_0 + \beta_1 x_{i1} + \beta_2 x_{i2} + \beta_3 x_{i3} + \varepsilon_i$$

β_0, β_1, β_2, β_3 are all regression parameters

Where i =1 to *n*

$\varepsilon_i \sim N(0, \sigma^2)$.

iid

Where Y_i represents the mean compressive stress for a given tear strength (x_1), flexural strength (x_2), and basis weight. (x_3). Table 4.7 displays analysis of variance for the regression model.

Table 4.7 Analysis of Variance of Regression Model

Source	DF	Sum of Squares	Mean Square	F-Value	P-Value
Model	3	225.9403	75.31348	91.38	0.0019
Error	3	2.47265	0.82422		
Total	6	16.29182			

Root MSE	0.90786
R-Square	0.9892
Coefficient of variation	16.29182

Under the null hypothesis (H_o), all regressions coefficients equal zero, implying that all independent variables, i.e. tear strength, (x_1), flexural strength (x_2), and basis weight. (x_3) have no linear association on the dependent variable, compressive stress. At 95-% confidence the null hypothesis is rejected and a linear association is concluded (p=0.0019). A reported R-square value of 0.9892 indicates the model fits well with the data.

Table 4. 8 displays the partial estimated regression coefficients for the regression model proposed. Flexural strength is observed to have a positive linear association with compressive stress (p=0.062). Tear strength (β_1) and basis weight (β_2), do not display a strong linear association with compressive stress based on the partial estimated regression coefficients (p= 0.4327 and 0.7721), respectively. However, table 4.9 reports correlation coefficients of 0.8158 and 0.90347 for tear strength and basis weight, respectively.

Table 4.8 Partial Regression Coefficients

Variable	DF	Estimate	Standard	t-value	p-value
Intercept (β_0)	1	2.08980	1.22422	1.71	0.1856
Tear strength (β_1)	1	-0.04347	0.04809	-0.09	0.4327
Flexural strength (β_2)	1	4.97215	0.71829	6.92	0.0062
Basis Weight (β_3)	1	0.00440	0.01389	0.32	0.7721

It is observed that the flexural properties have a greater impact on the compressive stress of three-dimensional structures from nonwovens than tear strength and basis weight (this assumption is also evidences by the 0.9929 correlation coefficient recorded in table 4.9). Specifically, the stiffer the substrate prior to thermoforming, the greater the compressive stress the resultants structure will provide.

Table 4.9 Pearson Correlations Coefficients

	Compressive Stress (y_1)
Tear strength (x_1)	0.8158 (p=0.253)
Flexural strength ($x_{2)}$	0.99296 (p<0.0001)
Basis Weight (x_3)	0.90347 (p=0.0053)

5. Experimental Work: The Effect of Processing Parameters on Maximum Deformation

5.1 Factors and Response Variable

A 50-Ton hydraulic press was utilized for initial molding trials and is displayed schematically in Figure 2.

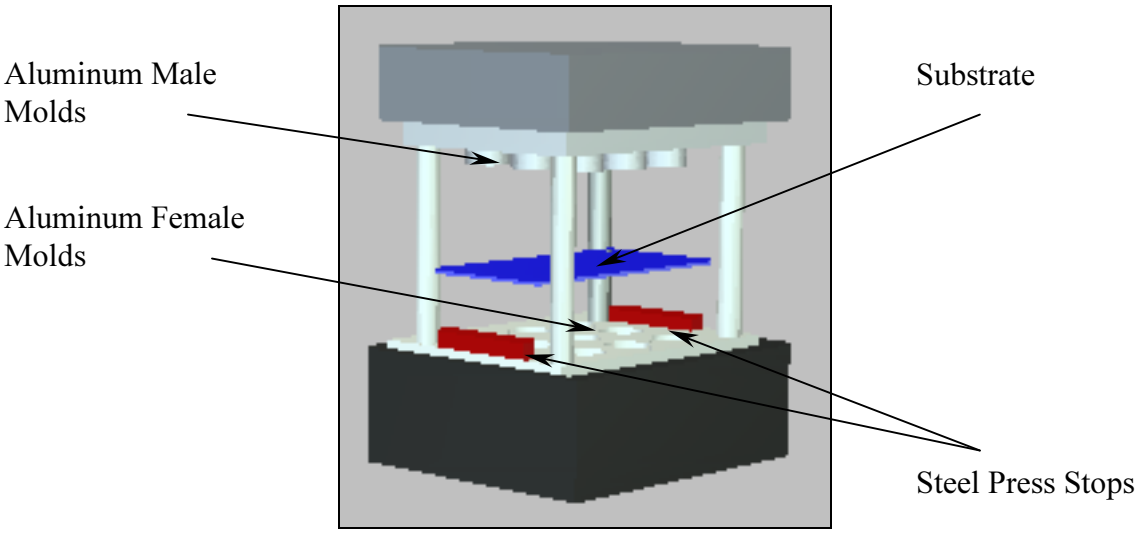

Figure 5.1 SpaceNet Hydraulic Press

5.2 Operating Temperature

Operating temperature (T) is the temperature at which substrate molding will occur. Through the application of heat molecular movement is induced within the polymer thus softening the fiber. This fiber softening allows deformation to occur at lower stress levels compared the stress levels required to deform the fiber when processed at ambient temperatures (15˚ - 30˚ C). To maintain fibrous characteristics without considerable change to molecular orientation and crystallinity, a forming temperature (operating temperature) above, but closer to glass transition and below the melting temperature is used. For polyester fibers (which make up the polymer content of

the substrates used in this study) the glass transition temperature and melting temperature are 120˚C and 260˚C, respectively.

5.3 Residence and Molding Times

Residence time (R) is defined as the time permitted for *substrate preheating* to occur in this molding process. Residence time should be sufficient to induce and allow for the molecular movement and the subsequent fiber softening described previously. Because a direct preheating chamber is not available, machine design dictated preheating the substrate by lowering the press to the point where the heated male and female molds are in direct contact with the substrate. The time that the press is in the lowered position before deformation occurs is recorded as residence time (in seconds). We assume that the heated molds resting on the surface of the substrate would allow for adequate thermal transfer and induce fiber softening. After preheating is complete (as defined by residence time) the press is completely lowered to induce substrate deformation. Mold time (M) is therefore measured as the time the substrate is in the deformed state. It is important to note that 'mold time' should be sufficient to set the substrate into its deformed state. Insufficient mold times will produce products that will not retain their respective shapes (i.e. three-dimensional effect).

5.4 Response Variable: Maximum deformation

To evaluate how a particular substrate will respond to the given set of the processing conditions a method to deduce maximum deformation was developed. From previous work it was found that that steel press stops (refer to figure 5.1 above) limit the depth of penetration through the substrate achieved by the male mold. Stop height in this respect is defined as the measured height (mm) of the steel press stops used. Stop heights

are adjustable and can be varied to achieve maximum deformation achieved for the substrate used in this study. Smaller stop heights allow the male mold to penetrate the female mold to a greater depth; thus in turn producing thicker projections on the substrate. Comparatively, large stop heights limit the depth achieved by the male mold, which in turn produces smaller/thinner projections rising from substrate plane. The smaller the stop heights the more deformation the substrate will undergo. Stop height therefore impacts formed product dimensions, specifically formed product thickness. It should be noted that there is a limit in regards to stop height, i.e. exceedingly low stop heights the will allow the male mold to completely penetrate the substrate, thus producing holes or a failure in processing.

The manipulation of stops heights will be the measurement tool used to evaluate maximum deformation or maximum-formed product thickness. It is proposed that for each treatment combination a series of stop heights will be used beginning with high stop heights (10 mm) and continuing with lower stops heights until the male mold penetrates the substrate. For example, for one treatment combination the initial stop height will be 10 mm and a sample will be produced, the next sample a stop height of 8 mm will be used, then 6mm. etc. At a particular stop height the male mold will completely penetrate the substrate surface producing holes (i.e. failure has occurred). The stop height and the relative substrate that produced the greatest product thickness before failure occurred will be used as a measure of maximum deformation (or product thickness measured in mm)

Factors R and T have three levels (0,1,2) and M has two levels (0,1). All treatment combinations in a complete crossed design are given below.

Table 5.1. Factors and Response Variables

Factor	**Levels**
T: Temperature (˚C)	160 (0), 175 (1), 190(2)
R: Residence Time (s)	15 (0), 45(1), 75 (2)
M: Mold Time (s)	10 (0), 40(1)
Response Variable	
Maximum Deformation	mm

Table 5.2 Treatment Combinations

Run	**T**	**R**	**M**	**Label**
1	0	0	0	$T_0R_0M_0$
2	0	0	1	$T_0R_0M_1$
3	0	1	0	$T_0R_1M_0$
4	0	1	1	$T_0R_1M_1$
5	0	2	0	$T_0R_2M_0$
6	0	2	1	$T_0R_2M_1$
7	1	0	0	$T_1R_0M_0$
8	1	0	1	$T_1R_0M_1$
9	1	1	0	$T_1R_1M_0$
10	1	1	1	$T_1R_1M_1$
11	1	2	0	$T_1R_2M_0$
12	1	2	1	$T_1R_2M_1$
13	2	0	0	$T_2R_0M_0$
14	2	0	1	$T_2R_0M_1$
15	2	1	0	$T_2R_1M_0$
16	2	1	1	$T_2R_1M_1$
17	2	2	0	$T_2R_2M_0$
18	2	2	1	$T_2R_2M_1$

5.5 Experimental Design

Eighteen total treatment combinations exist given the number of factors and levels for each factor. Because interactions may be important, all combinations of factors will be evaluated. A temperature adjustment on this specific press takes a substantial amount of time to heat up, cool and reheat. Given this constraint treatment combinations within a

given temperature should be completed consecutively. The proposed design groups 3 treatment combinations into six whole plots. Specifically, mold time and temperature will be grouped into whole plots. Reducing whole plots to a size of three will allow a degree of randomization of temperature to be accomplished. Therefore the randomization scheme will be as follows:

1. Group treatment combinations by temperature and mold time and randomize the run order of the respective residence times.
2. Randomize the order in which the whole plots (temperature and mold time groupings) will be run.

The following tables outline the run order for experimental design

Table 5.3. Randomized Run Order

Run	T	M	R	Label	Run	T	M	R	Label
1	0	1	2	$T_0M_1R_2$	10	0	0	2	$T_0M_0R_2$
2	0	1	1	$T_0M_1R_1$	11	0	0	1	$T_0M_0R_1$
3	0	1	0	$T_0M_1R_0$	12	0	0	0	$T_0M_0R_0$
4	2	0	2	$T_2M_0R_2$	13	2	1	0	$T_2M_1R_0$
5	2	0	0	$T_2M_0R_0$	14	2	1	1	$T_2M_1R_1$
6	2	0	1	$T_2M_0R_1$	15	2	1	2	$T_2M_1R_2$
7	1	1	1	$T_1M_1R_1$	16	1	0	1	$T_1M_0R_1$
8	1	1	2	$T_1M_1R_2$	17	1	0	2	$T_1M_0R_2$
9	1	1	0	$T_1M_1R_0$	18	1	0	0	$T_1M_0R_0$

5.5 Statistical Methods and Data

Analysis will include F-tests for main effects and two-factor interactions where appropriate. Interactions plots will be used to augment tests for effects. Treatment means, quadratic and linear contrasts will be included with standard errors. Because only one replicate was completed, the design confounds whole plots with mold time. The

implications of this on the analysis will be discussed below. Table 4 displays the data obtained.

Table 5.4 Response Data

Run	Label	T	M	R	Mean Max. Deformation (y)
1	$T_0M_1R_2$	0	1	2	6.5731429
2	$T_0M_1R_1$	0	1	1	6.1217143
3	$T_0M_1R_0$	0	1	0	6.0118571
4	$T_2M_0R_2$	2	0	2	7.9664286
5	$T_2M_0R_0$	2	0	0	6.7878571
6	$T_2M_0R_1$	2	0	1	7.5014286
7	$T_1M_1R_1$	1	1	1	6.7188571
8	$T_1M_1R_2$	1	1	2	6.8031429
9	$T_1M_1R_0$	1	1	0	6.7102857
10	$T_0M_0R_2$	0	0	2	5.519
11	$T_0M_0R_1$	0	0	1	6.1757143
12	$T_0M_0R_0$	0	0	0	5.7667
13	$T_2M_1R_0$	2	1	0	6.863
14	$T_2M_1R_1$	2	1	1	7.6952857
15	$T_2M_1R_2$	2	1	2	8.1027143
16	$T_1M_0R_1$	1	0	1	6.527
17	$T_1M_0R_2$	1	0	2	7.0852857
18	$T_1M_0R_0$	1	0	0	6.2118571

5.6.1 Statistical Analysis

5.6.1.1 Full Model

As described above a spilt-plot experimental design was used to evaluate the effect of temperature and residence time and mold time on maximum deformation. Note that one replicate was used thus providing the following (full) linear model:

$$Y_{ijk} = \mu + T_i + M_j + \delta_{ij} + R_k + (TR)_{ik} + (MR)_{jk} + \varepsilon_{ijk}$$

Where i =0,1,2, j=0,1 and k=0,1,2

$\delta_{ij} \sim N(0, \sigma^2_{\delta})$ $\varepsilon_{ijk} \sim N(0, \sigma^2)$.

iid iid

Where Y_{ijk} represents the observation from the i^{th} temperature at the j^{th} mold time at the k^{th} residence time. Additionally δ_{ij} & ε_{ijk} are random effects, all others (T, M, and R) are fixed.

5.6.1.2 ANOVA

To determine the presence of main effects and interactions F-Tests were conducted. The following table displays the ANOVA results for this experiment. (Note: Type I sums of squares are reported/full model).

Table 5.5 Analysis of Variance

Source	DF	Sum of Squares	Mean Square	F Value	P-Value
Temperature	2	6.40438922	3.20219461	81.96	0.0121
Mold Time	1	0.23546464	.23546464	6.03	.1335
Whole Plot	3	0.0781369	0.03906845	.34	0.7282
Residence Time	2	1.17202111	0.58601055	5.15	0.0781
Temperature*Residence Time	4	0.63798149	0.15949537	1.40	0.3754
Mold Time* Residence Time	2	0.03209102	0.01604551	0.14	.8725
Error	6	0.45474787	0.11368697		
Total	17	9.01483224			

To determine the presence of a temperature effect, the following F-ratio was used

$$F = \frac{MS(Temperature)}{MS(Whole)} = \frac{3.20219461}{0.03906845} = 81.96$$

An F-ratio of 81.96 (p =. 0101) as noted in table 5 and above suggests the presence of a temperature (T) effect among the data under 95% confidence. Therefore it is concluded that temperature will impact the maximum deformation achieved by a substrate.

Similar steps are taken to determine the presence of a mold time (M) effect. Calculating the appropriate F-critical value for mold time effect included using the whole plot error or mean square error in the F-ratio. Therefore the following relation was used:

$$F = \frac{MS(MoldTime)}{MS(Error)} = \frac{0.23546464}{0.03906845} = 6.03$$

With a reported F-ratio value of 6.03 (p=0.1355) the presence of a mold time effect is concluded insignificant with 95% confidence. Mold time therefore does not influence the maximum deformation achieved by a particular substrate. Above conclusions are consistent with assumptions made before experimentation. It was believed that mold time has little effect on product thickness and therefore maximum deformation based on the fact the measurement of mold time begins after substrate deformation has already occurred.

Determining the presence of a residence time (R) effect involves calculating the appropriate F-critical value for residence time effect, which includes using the sub-plot error or mean square error in the F-ratio. Therefore the following relation was used

$$F = \frac{MS(\mathrm{Re}\,sidenceTime)}{MS(Error)} = \frac{0.586}{0.113} = 5.15$$

With a reported F-ratio value of 5.15 (p=0.0781) the presence of a residence time effect is concluded insignificant with 95% confidence. Residence time therefore does not influence the maximum deformation achieved by a particular substrate. Above conclusions are inconsistent with assumptions made before experimentation. While no residence time effect was established the p-value (0.0781) suggests that residence may influence maximum deformation, but not to extent where conclusions may deem it significant.

As described previously, whole plots are completely confounded with mold time. Therefore the test for the presence of a plot effect includes both mold time and the mold time*temperature interaction. Therefore the mold time*temperature interaction is not estimable. Fore reason described above (whole plots confounded with mold time) the only tests for the two-factor interactions that can be completed are the mold time and residence time and residence time and temperature interactions. Testing for the presence of a Residence Time * Temperature Interaction involves utilizing the following F-ratio:

$$F = \frac{MS(\text{Re}\,sidenceTime * Temperature)}{MS(Error)} = \frac{0.15949537}{0.113} = 1.40$$

From table 5 above this ratio has a value of 1.40 (p=0.3750) indicating the lack of a Residence Time * Temperature interaction (with 95% confidence). Testing for the presence of a mold time*residence time interaction involves using the following relation:

$$F = \frac{MS(MoldTime * \text{Re}\,sidenceTime)}{MS(Error)} = \frac{0.01604}{0.113} = .140$$

The following interaction plot shows responses averaged over mold time.

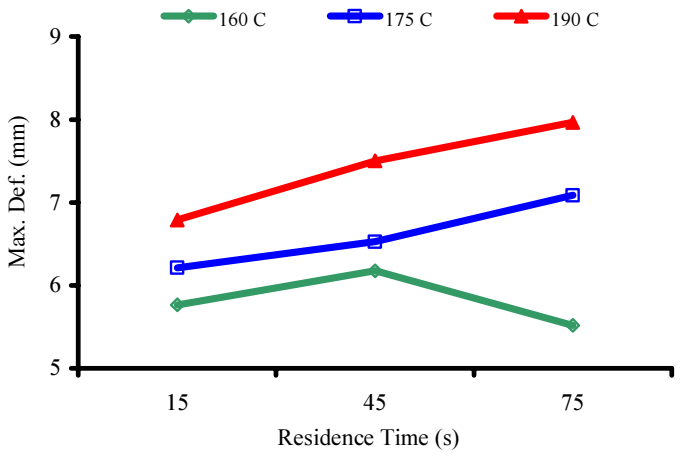

Figure 5.2 Interaction Plots of Residence Time and Temperature

The plot above shows that increases in temperature will increase the maximum deformation or product thickness for the substrate used. Additionally for higher temperatures (175˚C and 190˚C), increases in residence time will also increase the maximum deformation achieved. At the lowest temperature used (160˚C), initial increases in maximum deformation are observed followed by a decrease at the highest residence time. It should be noted that no significant interactions were observed in the statistical analysis conducted.

5.6.1.2 Factor Means

The following table displays the factor level means for all estimable factors

Table 5.6 Residence Time (Level Means)

Temperature (˚C)	Max. Deformation (mm)
160 (0)	6.028 (0.1961)
175 (1)	6.676 (0.1961)
190 (2)	7.486 (0.1961)

Table 5.7 Temperature (Level Means)

Residence Time (s)	Max. Deformation (mm)
15 (0)	6.3919 (0.1595)
45 (1)	6.7900 (0.1595)
75 (2)	7.0082 (0.1595)

5.6.1.3 Linear and Quadratic Contrasts

The linear and quadratic effects of both temperature and residence time were estimated. Estimating the linear effect of temperature with maximum deformation is given by the following contrast:

$$\overline{Y}_{2..} - \overline{Y}_{0..} = 7.846 - 6.028 = 1.458$$

$$SE(\overline{Y}_{2..} - \overline{Y}_{0..}) = \sqrt{\frac{2(MS(Whole))}{6}} = \sqrt{\frac{2 * 0.039}{6}} = 0.114$$

Linear Temperature Effect: 1.458 (0.114)

The value reported here suggests that a positive linear trend characterizes the relationship between temperature and maximum deformation. Estimating the linear effect with respect to residence time however is given by the following contrast:

$$\overline{Y}_{.2} - \overline{Y}_{.0} = 7.0082 - 6.3919 = 0.6163$$

$$SE(\overline{Y}_{.2} - \overline{Y}_{.0}) = \sqrt{\frac{2MS(Error)}{12}} = \sqrt{\frac{2 * 0.1136}{12}} = 0.1375$$

Linear Residence Time Effect: 0.6163 (0.1375)

As with temperature, a positive linear relationship between residence time and maximum deformation is suggested by the values reported above.

To estimate the presence of a quadratic effect for temperature the following contrast is used.

$$(\overline{Y}_{0..} - 2\overline{Y}_{1..} + \overline{Y}_{2..}) = 6.028 - 2(6.676) + 7.486 = 0.162$$

$$SE(\overline{Y}_{0..} - 2\overline{Y}_{1..} - \overline{Y}_{2..}) = \sqrt{MS(Whole)} = \sqrt{0.039} = 0.1974$$

Quadratic Temperature Effect: 0.162 (0.1974)

The lack of a quadratic effect temperature suggested by the data supports the assumption of that a linear effect is present for temperature.

Estimating the presence of a quadratic effect for residence time follows in a similar manner. The following contrast is used.

$$(\overline{Y}_{..0} - 2\overline{Y}_{..1} + \overline{Y}_{..2}) = 6.3919 - 2(6.79) + 7.0082 = -0.1799$$

$$SE(\overline{Y}_{..0} - 2\overline{Y}_{..1} - \overline{Y}_{..2}) = \sqrt{MS(Error)} = \sqrt{0.1136} = 0.337$$

Quadratic Residence Time Effect: -0.1796(0.337)

The lack of a quadratic effect of residence time is also suggest suggested by the data and additionally supports the conclusion that a linear effect is present for residence time.

5.7 Conclusions

Based on the experimental work and statistical analysis completed to date the following conclusions come forth.

- Temperature has been shown to affect (increase) the maximum deformations of nonwoven substrates.
- Residence time has been shown not affect the maximum deformation of nonwoven substrates.
- Mold time has been shown not to affect the maximum deformation of nonwoven substrates.
- The presence of an interaction between temperature and residence time has not been established.
- The presence of an interaction between mold time and residence time has not been established
- Due to the lack of a residence time effect and a temperature*residence time interaction it can be concluded that temperature and residence time effect maximum deformation independently (i.e. increases in product thickness can be achieved via adjustments in temperature alone).
- Due to whole plot confounding with mold time the presence or lack thereof of mold time*temperature and other higher order interactions (three factor interactions) cannot be determined with confidence.
- The effect of temperature on maximum deformation can be described as a positive linear relationship.
- The effect of residence time on maximum deformation can be described as a positive linear relationship but the residence time effect is not significant.

6. The Effect of Mold Geometry on Compressive Properties

Apparent affects of adjustments in mold geometry include changes in product dimension and form. What has been investigated in the current work was how adjustments in mold geometry translate into shifts in compressive properties of the formed products produced in this study. Pin diameter, a component of mold geometry, affects how much deformation is introduced to the specific substrate. In addition, it provides the simplest way to change final product dimension and form and will be used to describe mold geometry for the reminder of this thesis. Three pin diameters were used: ½", 3/8" and ¼", and all substrates (8 in total) were processed at each respective pin diameter.

6.1 Substrates

PET/CoPET spunbond webs were used and acquired from commercial sources. Basis weights ranged from 100 g/m^2 to 180 g/m^2. Mechanical tests were conducted on all substrates and data is reported in table 6.1. Note the relatively isotropic tensile properties of the substrates.

Table 6.1 Substrate Properties

Sample	g/m^2	Fiber Type	Strain at Break MD/CD	Peak Tensile Load (kgf) MD/CD
2295	100	PET	62.1/64.8	9.3/12.3
2033	100	PET	42.1/48.3	12.2/7.8
052-100	100	PET/CoPET	30.21/34.57	9.9/7.9
052-140	140	PET/CoPET	32.9/37.7	15.12/10.96
052-180	180	PET/CoPET	37.7/38.25	20.7/16.6
072-100	100	PET/CoPET	30.42/35.1	6.2/5.5
072-180	180	PET/CoPET	40.40/40.35	13.76/14.24
056-130	130	PET/CoPET	27.6/33.9	11.05/11.14

Nonwoven fabric proprieties follow fiber orientation with great reliability. Therefore, it can be surmised that the isotropic tensile properties observed in Table 1 indicate a

relatively uniform fiber orientation distribution. The orientation distribution functions of the substrates are reproduced in figure 6.1. Note the relatively uniform fiber orientation that precludes isotropic tensile properties. Previous work reported in this thesis indicated that webs comprised of more uniform fiber orientations also have uniform directional strain to break values, which improves substrate moldability. This "moldability" is pertinent only when utilizing this particular type of mold (cylindrical pins)[4].

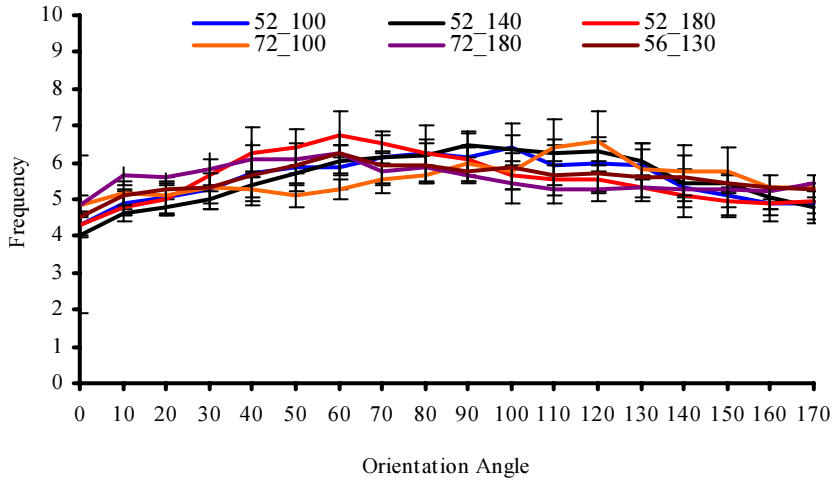

Figure 6.1 Fiber Substrate Orientation Distributions

6.2 Compressive Properties

The compressive properties were measured for each of the substrates formed at the three pin diameters described above. Because no standard test method exists for evaluating the compressive properties of three dimensional fiber networks, a method was derived and includes the following test parameters:

- Platen separation: 10 mm
- Crosshead speed: 1mm/min to 40% strain
- Specimen thickness: Taken at .005 kgf
- Machine type: CRE

A standard Instron tensile testing device was used.

Compressive stress (σ_c ,psi) was calculated by using the following relation.

$$\sigma_C = F/A, \quad (5)$$

Where F is the peak force (lb-f) required to compress product to 40% strain and A is the total area (in^2) that the platen is in contact with the formed product. Total area A is the calculated area of the dome (projection) tops in the structure produced (note that this value changes for different pin diameters).

Referring to figure 6.2, it is observed that increases in pin diameters are associated with decreases in compressive stress. Statistical analysis concludes that pin diameter effects are significant ($p < 0.0001$, table 6.2). Larger pin diameters (i.e. 1/2" pin diameter) will increase the surface area from that on the initial substrate to a greater extent than small pin diameters (1/4"). The result is a lower mass density at projection tops for larger pin diameters; consequently, the lower mass density has a detrimental effect on compressive properties. The opposite would be true for small pin diameters; mass density is maintained because overall deformation is minimized (products formed from small pin diameters have a smaller thickness (draw ratios) than products formed using larger pin diameters) therefore compressive stress is greater. Additionally, fewer domes are produced for a given product area for large pin diameters compared to small pin diameters. Therefore larger pin diameters have the effect of reducing the number of supporting columns available for compressive resistance.

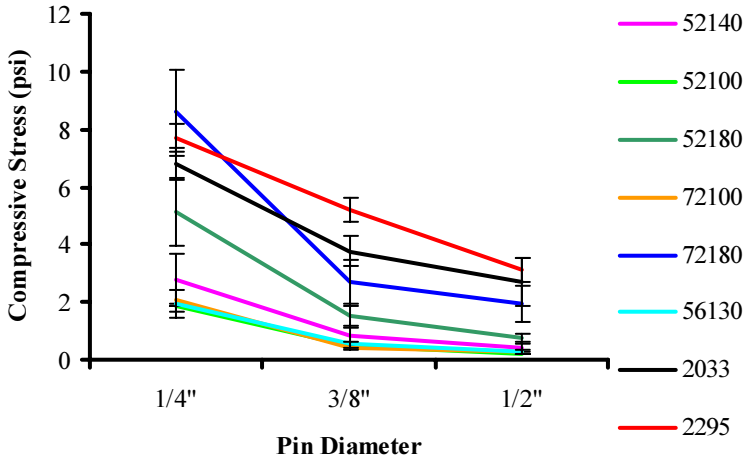

Figure 6.2 Effect of Pin Diameter on Compressive Peak Stress

An analysis of variance supported the inferences made from graphical observation.

Table 6.2 ANOVA for Compressive Stress Data

Source	DF	Sum of Squares	Mean Square	F Value	P-Value
Pin Diameter	2	338.67	169.33	34.12	<. 0001
Web	7	769.28	109.89	22.14	<. 0001
Pin Diameter*Web	14	124.26	8.8759	1.788	0.0438
Error	168	833.72	4.96		
Total	191	2065.95			

A web (substrate) effect has also been concluded significant ($p < 0.001$) at 95-% confidence. This reveals that different substrates will provide for different compressive stress. This conclusion is apparent when one examines the range of physical characteristics observed for the substrates utilized in this thesis (refer to table 6.1). Additional conclusions rest on the presence of an interaction between web (substrate) and pin diameter ($p=0.0438$). Compressive properties associated with changes in pin diameter vary from substrate to substrate and from one pin diameter another. Referring to Appendix C, homogeneity of variances and normality is concluded. From the previous conclusion it follows that inherent web (substrate) characteristics (polymer type, basis

weight, degree/level of bonding) greatly influence the compressive properties of formed three-dimensional structures.

The compressive secant modulus was calculated between 0-% and 15-% strain for all substrates produced. By convention, the secant modulus is calculated based on the rate of in addition to the typical strains that will be expected during product specific end-use. The compressive secant modulus to 15- % strain was selected based on observation that up to15% strain, the rate of loading has increased significantly from 0-% strain for all substrates evaluated. Thus, secant modulus to 15-% strain becomes a material property only useful in comparing one product to another. Figure 6.3 displays the effect of pin diameter on compressive secant modulus.

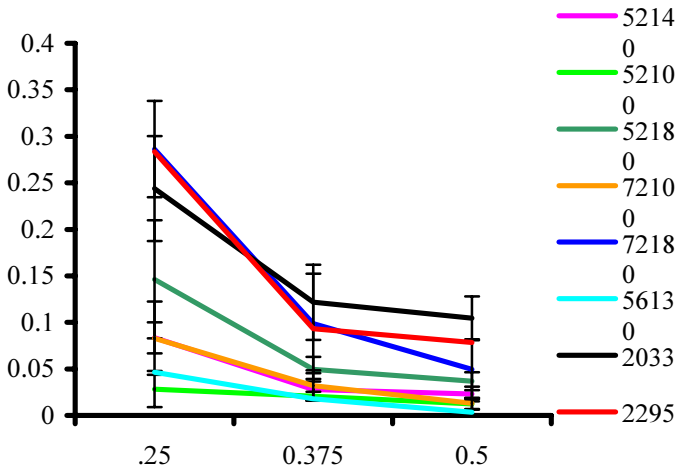

Figure 6.3 Effect of Pin Diameter on Compressive Secant Modulus.

Referring to figure 6.3, it is observed that increases in pin diameters are associated with decreases in compressive modulus. Statistical analysis concludes that pin diameter effects are significant ($p < 0.0001$, table 6.3). (Referring to Appendix C, homogeneity of variances and normality is concluded). Larger pin diameters (i.e.1/2") will increase the surface area from that on the initial substrate to a greater extent than small pin diameters

(1/4”). Fewer domes are produced for a given product area for large pin diameters compared to small pin diameters. Therefore larger pin diameters have the effect of reducing the number of supporting columns available for compressive resistance.

Table 6.3 Analysis of Variance for Compressive Secant Modulus

Source	DF	Sum of Squares	Mean Square	F-Value	P-Value
Pin Diameter	2	0.28067	0.140335	113.5239	< 0.0001
Substrate	7	0.576185	0.082312	66.58642	< 0.0001
Pin Diameter * Substrate	14	0.394557	0.028183	22.79836	< 0.0001
Error	168	0.207677	0.001236		
Total	191	1.459089			

Similar observations were made form compressive secant modulus as were made for compressive stress. A pin diameters and substrate effects have been concluded significant ($p< 0.001$) at 95-% confidence. Interactions between web and pin diameters are also concluded significant ($p<0.001$). It can be surmised that compressive modulus associated with changes in pin diameters vary from substrate to substrate and from one pin diameter to the next.

Compressive-recovery curves were used to determine the total compressive energy, recovered energy and hysteresis of all samples. A typical curve is given below (Figure 6.4). Total compressive energy to 40% strain was taken as the total area under the compression curve (given in kj/m^2). Recovered energy was taken as the total area under the recovery curve (also given in kj/m^2). Hysteresis therefore was defined as the difference between total compressive energy and recovered energy (forthcoming graphs also show hysteresis as a percent of total energy consumed during one loading and unloading cycle).

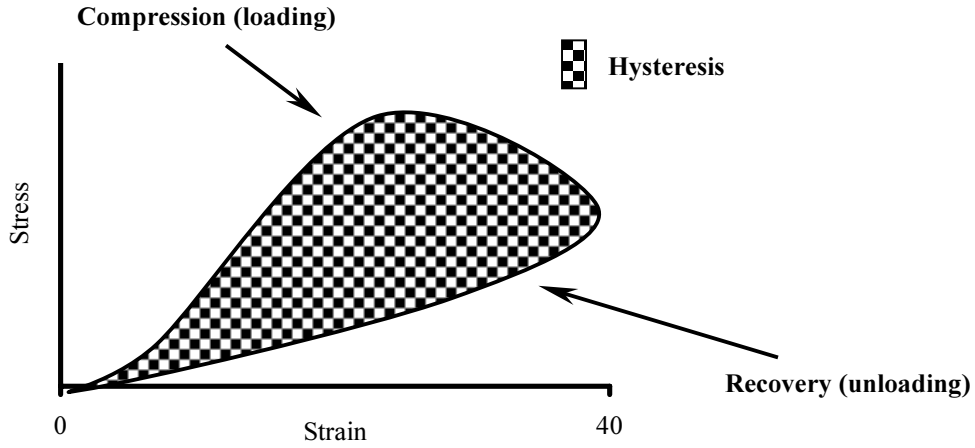

Figure 6.4 Typical Compression-Recovery Curve

Figure 6.5 displays total compressive energy to 40-% as a function of pin diameter. If all webs are aggregated together, increases in pin diameter is known to decrease the total energy required to deform the product to 40% strain.

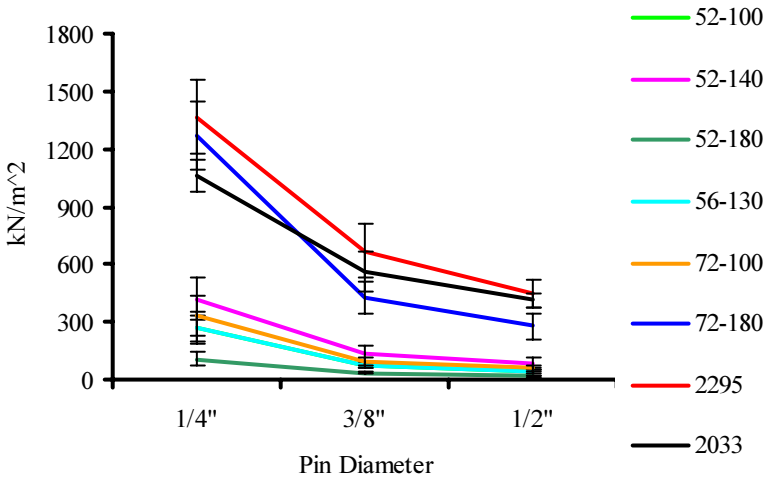

Figure 6.5 Total Compressive Energy to 40% Strain

Statistical analysis concludes that pin diameter effects are significant ($p < 0.0001$), table 6.4). A substrate effect is also observed ($p < 0.001$) at 95-% confidence. This reveals that differed substrates will provide for different compressive total energies. Additional conclusions rest on the presence of an interaction between web and pin diameter ($p = 0.0438$).

Table 6.4 Analysis of Variance for Total Energy

Source	DF	Sum of Squares	Mean Square	F-Value	P-Value
Pin Diameter	2	7827330	3913665	572.3071	< 0.0001
Substrate	7	16050795	2292971	335.3081	< 0.0001
Pin Diameter * Substrate	14	3689273	263519.5	38.53526	< 0.0001
Error	168	1148851	6838.4		
Total	191	28716249			

It can be surmised that compressive properties associated with changes in pin diameters vary from substrate to substrate and from one pin diameter to the next. The trend observed for total energy follows expected results due to the relationship between total energy and compressive stress (σ_c).

Recovered energy will also decrease with increases in pin diameter (Figure 6.6). Again. Further observation reveals that formed products are *recovering* from compressive forces in a different manner than they were loaded (compressed).

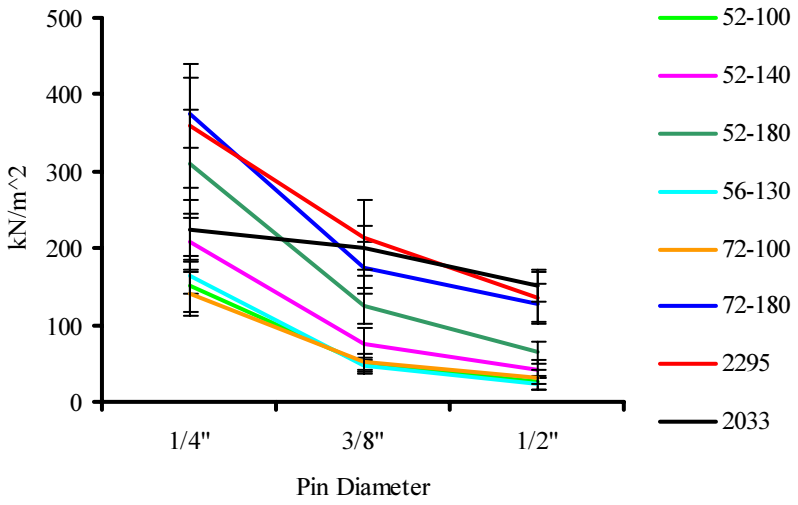

Figure 6.6 Recovered Compressive Energy

Table 6.5 Analysis of Variance for Recovered Compressive Energy

Source	DF	Sum of Squares	Mean Square	F-Value	P-Value
Pin Diameter	2	1406687	703343.6	48.32348	< 0.0001
Substrate	7	790418.4	112916.9	7.757997	<0.0001
Pin Diameter * Substrate	14	361830	25845	1.77569	0.045874
Error	168	2445224	14554.9		
Total	191	5004160			

Statistical analysis concludes that pin diameter effects and substrate effects are significant ($p < 0.0001$ for both main effects, Table 6.5). This reveals that different substrates will undergo different recovery mechanisms when subject to a compressive loading-unloading cycle. Additional conclusions rest on the presence of an interaction between web and pin diameter ($p = 0.045874$). This is attributed to the differences in inherent properties of the substrates, which are dictated by different processing conditions at substrate manufacture.

Hysteresis, or total energy exerted during one loading-unloading cycle is also dependent upon pin diameter (Figure 6.7).

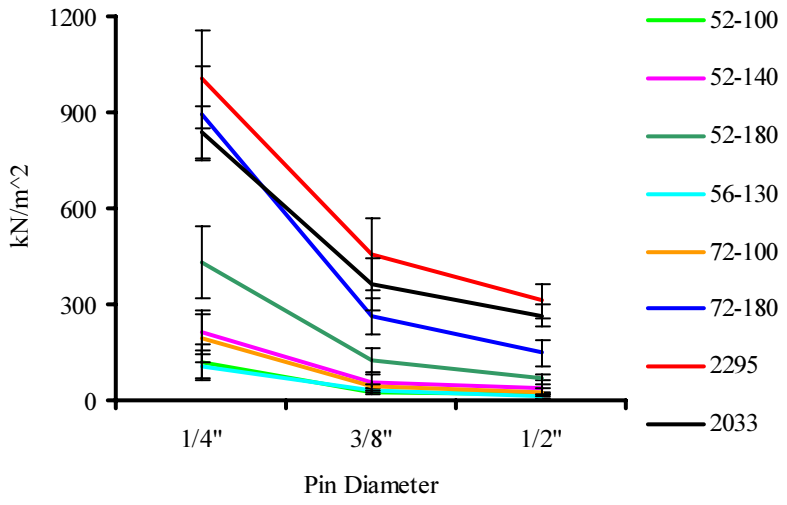

Figure 6.7 Hysteresis

Table 6.6 Analysis of Variance for Hysteresis

Source	DF	Sum of Squares	Mean Square	F-Value	P-Value
Pin Diameter	2	5280488	2640244	314.0425	< 0.0001
Substrate	7	7951253	1135893	135.1083	< 0.0001
Pin Diameter * Substrate	14	2377493	169820.9	20.19926	< 0.0001
Error	168	1412424	8407.283		
Total	191	17021657			

Analysis of variance also concludes that pin diameter and substrate effects are significant ($p < 0.0001$ for both main effects, Table 6.6). This reveals that energy loss during one compressive loading-unloading cycle varies from substrates to substrate. An interaction between substrate and pin diameter ($p = 0.045874$) is also observed.

Hysteresis, when taken as a percent of total energy gives the fraction of total energy required to complete one loading-unloading cycle relative to the total energy required to compress the product to 40% strain. Large values for hysteresis as a percent of total energy indicate that a greater fraction of energy is lost in one loading-unloading

cycle compared to smaller values for hysteresis as a percent of total energy. The *inability* of a formed product to recover compressive energy exerted is indicative of poor resiliency. Therefore, poor resilience is associated with large values for hysteresis as a percent of total energy.

Observing hysteresis as a percent of total energy, no overall pin diameter effect can be observed (Figure 6.8). Figure 6.8 shows that pin diameter does not dictate resilience, but inherent web (substrate) properties play a important role. However, note that pin diameter will alter the resiliency of individual formed products. This can be observed by referring to table 4 in appendix A and observing that the ascending order for hysteresis as percent of total energy changes from one pin diameter to another pin diameter.

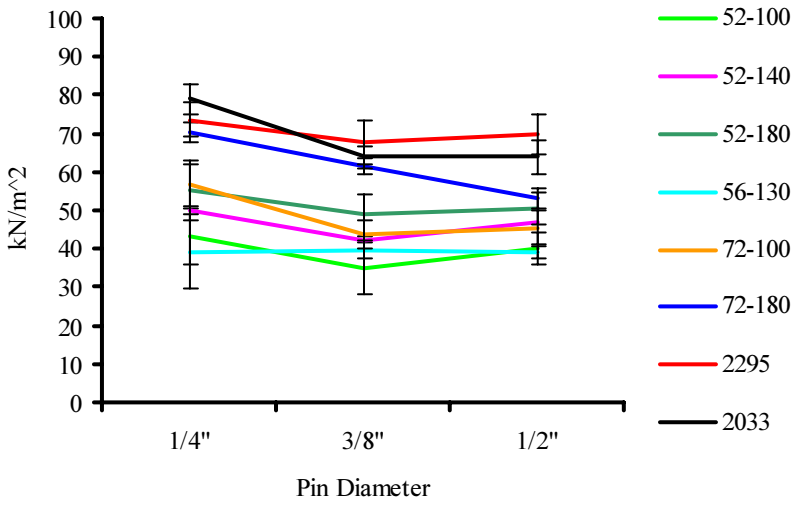

Figure 6.8 Hysteresis as a % of Total Energy

Table 6.7 Analysis of Variance for Hysteresis as a % of Total Energy

Source	DF	Sum of Squares	Mean Square	F-Value	P-Value
Pin Diameter	2	1842.085	921.0427	5.428006	0.005196
Substrate	7	26105.26	3729.322	21.97812	< 0.0001
Pin Diameter * Substrate	14	3615.91	258.2793	1.522124	0.107766
Error	168	28506.82	169.6834		
Total	191	60070.07			

Statistical analysis reveals that pin diameter ($p=0.005$) and substrate ($p < 0.0001$) effects are significant at 95-% confidence (Table 6.7). The presence of an interaction between pin diameter and substrate is not concluded ($p=0.10776$). This conclusion has several implications. One can now assume that specific mold geometry and substrate do not interact to impact hysteresis as a percent of total energy. Therefore resiliency can be engineered via substrate selection or mold geometry independent of one another.

6.1 Compressive Properties and the Level of Bonding

One hypothesis that may explain the phenomenon of resiliency relates to the "degree/level of bonding" of substrates prior to thermoforming and how these properties translate into formed product properties. Because a direct measure of the "level of bonding" is not easily attained, substrate flexural and tear properties were assessed. The assumption here is that the degree (or amount) of bonding is a material characteristic that impacts (either positively or negatively) stiffness (flexural strength) and tear strength. Tear strength was measured via the trapezoid method [71]. Flexural strength was measured via four-point bending [72] utilizing two loading noses that impact *and bend* a substrate sample that rests upon two supporting noses. A load–extension curve is therefore produced. For elastic materials catastrophic failure does not occur. Therefore *peak* load was used as a measure of flexural strength when bending a given sample.

Figures 6.9 and 6.10 display the tear and flexural properties for all substrates used in this study.

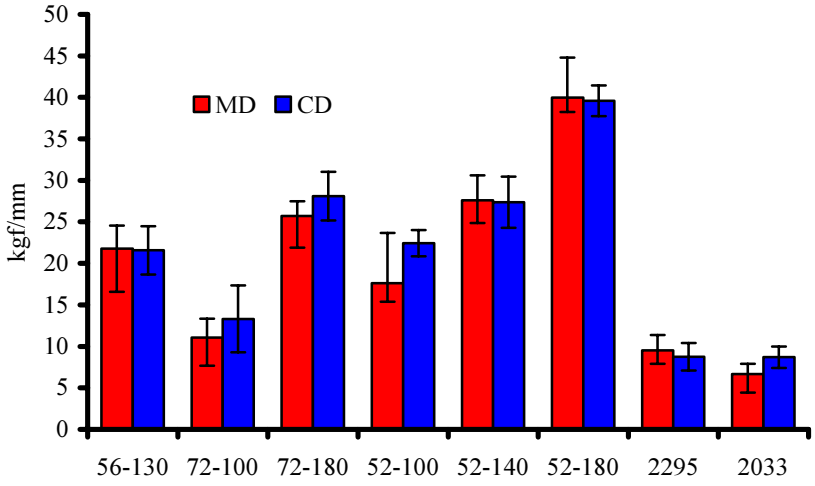

Figure 6.9 Substrate Tear Strength

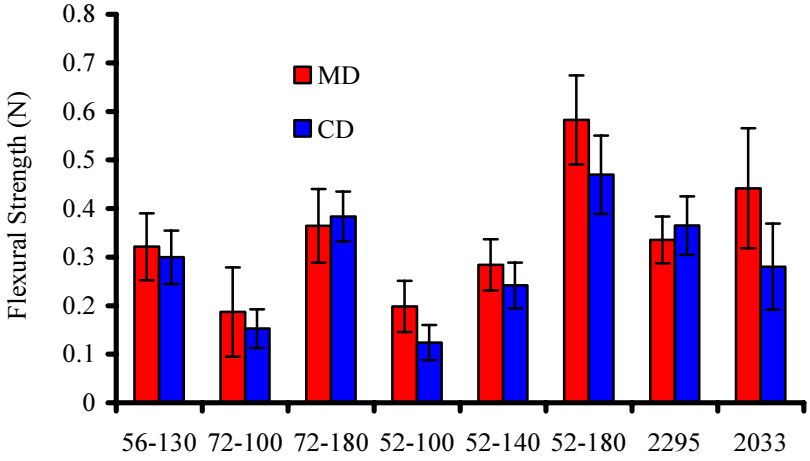

Figure 6.10 Substrate Flexural Strength

Figure 6.11 displays total compressive energy for all pin diameters used as a function of substrate tear strength (average between MD and CD tear strength is reported). A large variance in total compressive energy as a function of tear strength is observed. This result is expected due to large differences in total compressive energies for different pin diameters. However as the pin diameter increases a stronger correlation is observed (refer

to table 6.8). It should be noted this correlation does not imply causation and that –0.475 is still a poor indicator of linearity.

Table 6.8 Correlation between Tear Strength and Total Energy as a function of Pin Diameter

Pin Diameter	Correlation Coefficient of Total Energy and Tear Strength
1/4"	-0.2462615
3/8"	-0.4046022
1/2"	-0.4754783

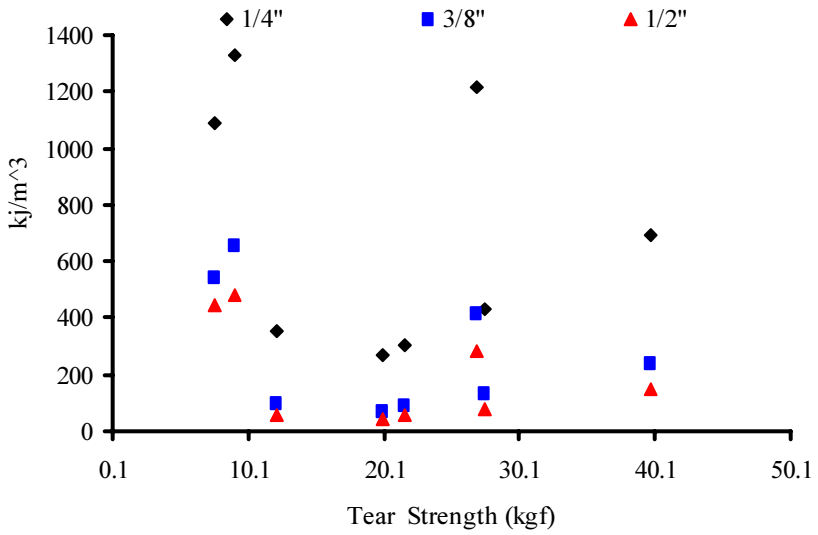

Figure 6.11 Tear Strength vs. Total Compressive Energy to 40% Strain

Recovered energy displays no strong linear association to tear strength (Figure 6.12, table 6.9). Correlation coefficients of 0.101377, -0.322 and -0.326955 were recorded for 1/4", 3/8" and 1/2" pin diameters, respectively. It is therefore concluded that no considerable change in correlation coefficients as function of pin diameter is observed (Table 6.9).

Table 6.9 Correlation between Tear Strength and Recovered Energy a function of Pin Diameter

Pin Diameter	Correlation Coefficient
1/4"	0.1013777
3/8"	-0.3223158
1/2"	-0.3262955

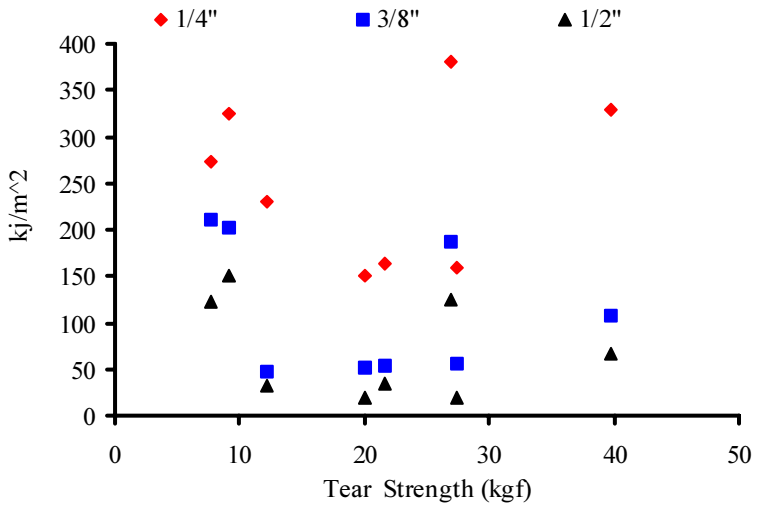

Figure 6.12 Recovered Energy

Observing hysteresis as a function of tear strength (Figure 6.13), stronger correlation coefficients are revealed as function of pin diameter compared to the data reported for total and recovered energy (refer to table 6.9, 6.10). For example, it is observed that as the pin diameters increase, tear strength better correlates to hysteresis. It should be noted that a –0.52 correlation coefficient reported for the ½" pin diameter is still a week correlation and causation cannot be concluded.

Table 6.10 Correlations between Tear Strength and Hysteresis a Function of Pin Diameter

Pin Diameter	Correlation Coefficient
1/4"	-0.3196582
3/8"	-0.4414711
1/2"	-0.5243115

Graphical observations reveal that no conclusive statements regarding hysteresis as function tear strength can be made.

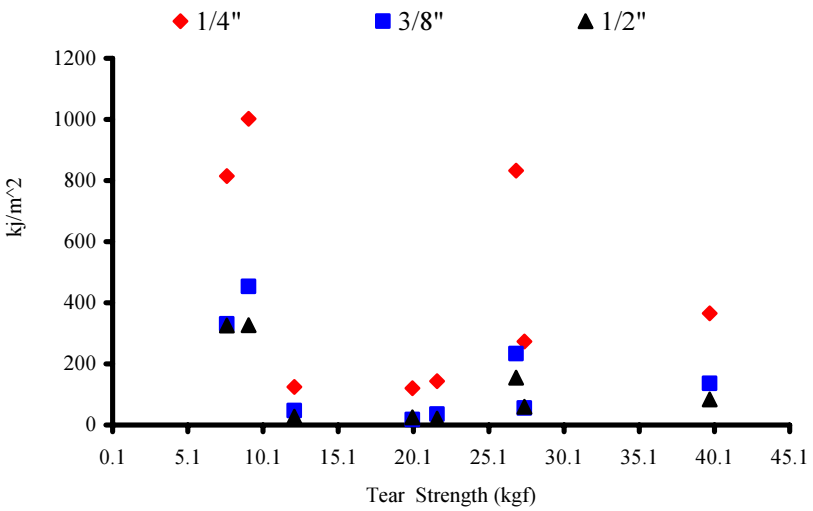

Figure 6.13 Hysteresis as a function of Tear Strength

Hysteresis, when taken as a percent of total energy gives the fraction of total energy required to complete one loading-unloading cycle relative to the total energy required to compress the product to 40% strain. Large values for hysteresis as a percent of total energy indicate that a greater fraction of energy is lost in one loading-unloading cycle compared to smaller values for hysteresis as a percent of total energy. The *inability* of a formed product to recover compressive energy is indicative of poor resiliency. Therefore, poor resilience is associated with large values for hysteresis as a percent of total energy. Examining the effect of tear strength of substrates on resilience no distinct relationship comes forth (refer to Figure 6.14).

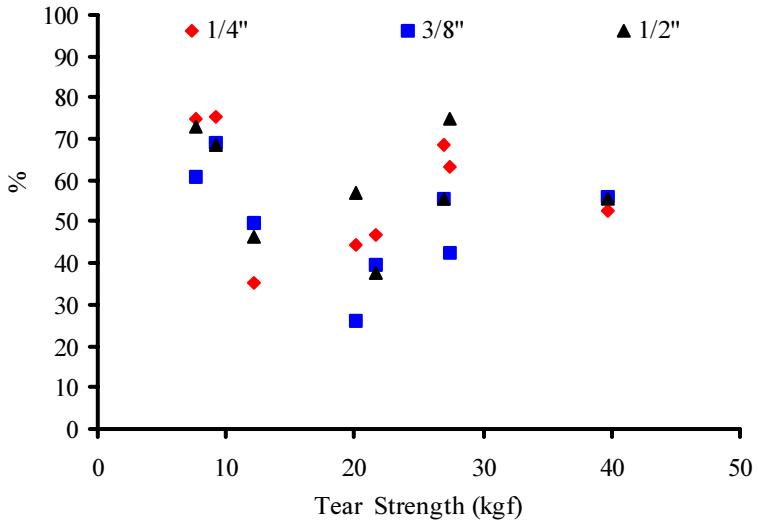

Figure 6.14 Hysteresis as a % of Total Energy Vs. Tear Strength

Table 6.11 Correlations between Tear Strength and Hysteresis as a % of Total Energy as a Function of Pin Diameter

Pin Diameter	Correlation Coefficient
1/4"	-0.2004582
3/8"	-0.2529579
1/2"	-0.18633

Figure 6.15 displays total compressive energy for all pin diameters used versus substrate flexural strength (average between MD and CD flexural strength is reported). A large variance in total compressive energy as a function of flexural strength is observed. This result is expected due to large differences in total compressive energies for different pin diameters. However stronger correlations between total energy and flexural strength compared to the correlations between total energy and tear strength are observed (refer to table 6.8and 6.12, respectively).

Table 6.12 Correlation between Flexural Strength and Total Energy a function of Pin Diameter

Pin Diameter	Correlation Coefficient
1/4"	0.5521138
3/8"	0.4915755
1/2"	0.4479801

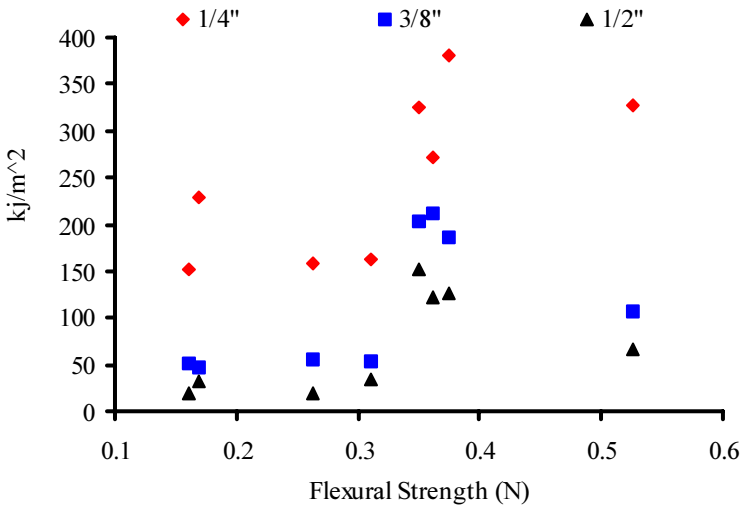

Figure 6.15. Total Compressive Energy to 40% Strain vs Flexural Strength

Recovered energy displays a relatively strong linear association (0.6921) with flexural strength at ¼" pin diameter (Figure 6.16, table 6.13). While a 0.6921 correlation coefficient is low under normal statistical assumptions, for nonwoven applications this could be concluded a strong correlation. Correlation coefficients of 0.6921386, 0.54 and 0.54 were recorded for of 1/4", 3/8" and1/2" pin diameters, respectively. No trend is revealed that concludes that a linear association between flexural strength and recovered energy as improves as a function of pin diameter. It is therefore concluded that no considerable change in correlation coefficients as function of pin diameter is observed (Table 6.13).

Table 6.13 Correlation between Flexural Strength and Recovered Energy a function of Pin Diameter

Pin Diameter	Correlation Coefficient
1/4"	0.6921386
3/8"	0.5404975
1/2"	0.5408454

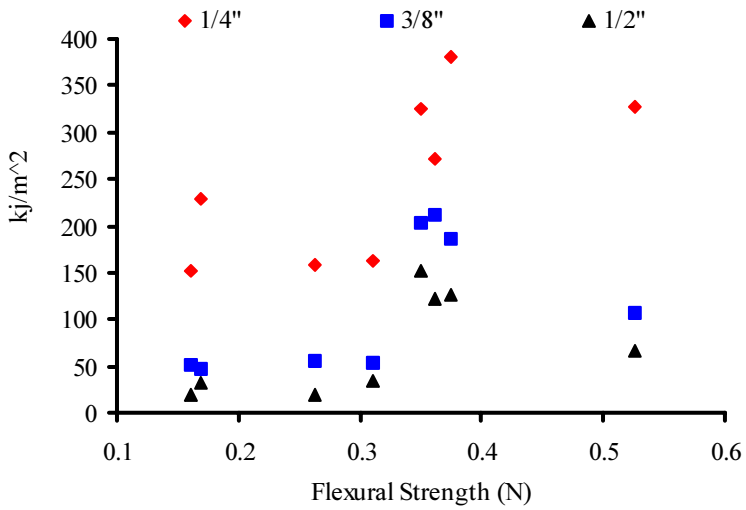

Figure 6.16 Recovered Energy Vs. Flexural Strength

Observing hysteresis as a function of flexural strength, weaker correlation coefficients are reported as function of pin diameter compared to the correlation coefficients reported for total and recovered energy (refer to table 6.14, 6.13, 6.12 respectively).

Table 6.14 Correlations between Flexural Strength and Hysteresis a Function of Pin Diameter

Pin Diameter	Correlation Coefficient
1/4"	0.4926989
3/8"	0.4619761
1/2"	0.3975277

Stronger correlations between hysteresis and flexural strength are observed compared to the correlations between hysteresis and tear strength (refer to table 6.14 and 6.9, respectively). Graphical observations (Figure 6.17) reveal that no conclusive statements regarding hysteresis as function flexural strength can be made.

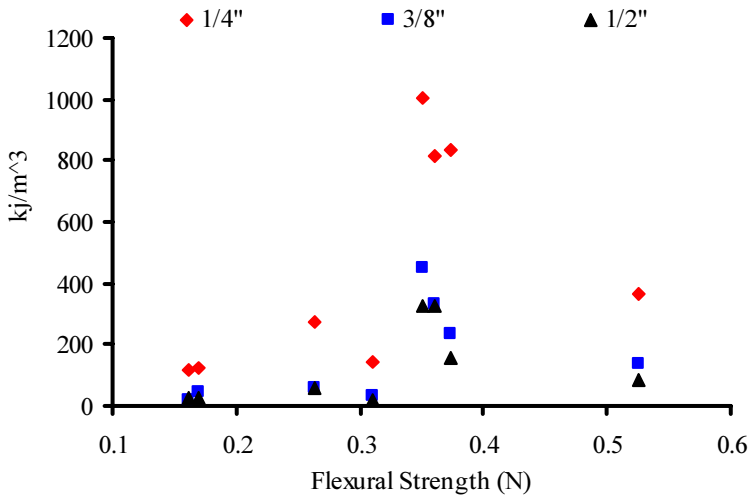

Figure 6.17 Hysteresis Vs. Flexural Strength

Hysteresis, when taken as a percent of total energy gives the fraction of total energy required to complete one loading-unloading cycle relative to the total energy required to compress the product to 40% strain. Large values for hysteresis as a percent of total energy indicate that a greater fraction of energy is lost in one loading-unloading cycle compared to smaller values for hysteresis as a percent of total energy. The *inability* of a formed product to recover compressive energy is indicative of poor resiliency. Therefore, poor resilience is associated with large values for hysteresis as a percent of total energy.

Below (Figure 6.18) resilience is displayed as a function of flexural strength. A slight relationship is revealed between flexural strength and resilience.

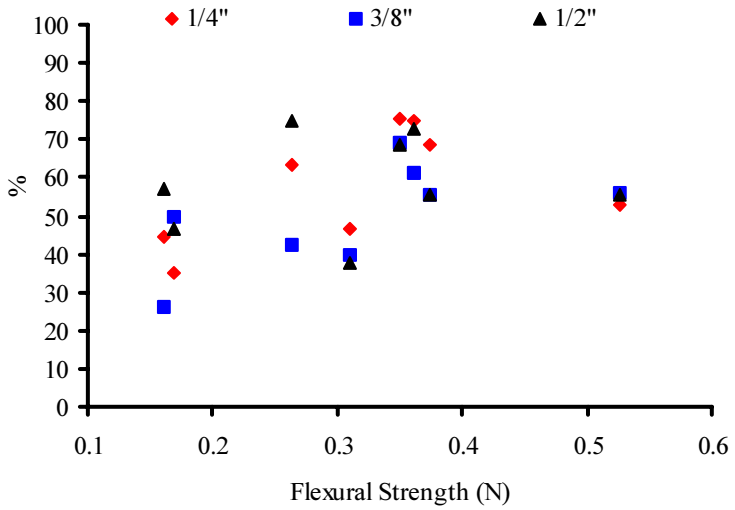

Figure 6.18 Hysteresis as a % of Total Energy Vs. Flexural Strength

Table 6.15 Correlations between Flexural Strength and Hysteresis as a % of Total Energy Function of Pin Diameter

Pin Diameter	Correlation Coefficient
1/4"	0.4849835
3/8"	0.6115185
1/2"	0.1336137

It can be observed that increases in flexural strength are associated with slight increases in hysteresis as a percent of total energy (or % energy loss). This indicates that stiff substrates will be less resilient when thermoformed into three-dimensional structures. The above graphs aggregates samples from all three-pin diameters utilized in this study, therefore supporting conclusions discussed above that inherent substrate properties play a large role in final product properties.

6.3 Conclusions

Based on the experimental work and statistical analysis completed to date the following conclusions come forth. Concerning the effect of the mold geometry the following conclusions were made

- Temperature has been shown to affect (increase) the maximum deformation of nonwoven webs.
- Decreases in pin diameters are associated with increases in compressive stress.
- Decreases in pin diameters are associated with increases in total compressive energy.
- Decreases in pin diameters are associated with increases in total recovered energy.
- Decreases in pin diameters are associated with increases in hysteresis.
- Mold geometry does not affect the resilience of formed products.
- The resilience of formed products improves with decreases in flexural strength.
- The resilience of formed products is not related to substrate tear strength.

7. Recommendations

The experimental results presented in this thesis attempted to add to the literature date regarding thermoforming deep-draw materials from nonwoven structures. Several conclusions presented above have come forth that outline processing guide for future work in this area. However several experimental aspects could have been added to the program to provide a more complete picture of the different issues involved in manufacturing three-dimensional structures from nonwovens. For example, the initial work described Chapter 4 attempted to understand substrates moldability and the mechanical deformation mechanisms involved. Understanding the biaxial deformation

mechanisms and how nonwoven processing conditions affect such mechanisms would prove beneficial. Additional work could include completing a strain-field analysis to understand to a greater degree the type of deformation a substrate will experience would also be very informative.

Regarding Chapter 5, the evaluation of how residence time (R) and operating temperature (T), and mold time (M) affect maximum deformation of nonwoven webs. The inability to complete two full replicates during experimentation limited a direct and complete realization the research objectives proposed. For example, the resulting confounding structure that surfaced during experimental design (i.e., mold time (M) is confounded with the plot effect) does not allow the interactions T*M and T*M*R to be estimable. Obviously, additional limitations imposed here include the inability to estimate linear and quadratic trends for mold time this in part due to the inability to make mold time estimates.

Overcoming the drawbacks with the current analysis outlined above with the aiming at fulfilling all research objectives can be achieved several ways. The completion of second full replicate of the current proposed design will allow the mold time to be estimable including any interactions in which with mold time is present. Other considerations include initiating a new experimental design that will still conform to constraints outlined early in the report but leave at minimum main effects and two factor interactions estimable.

The effect of mold geometry on compressive properties provides a great deal information. However future work could be concerned with investigating in more detail analysis of the “level of bonding” and its affect on formed product properties. Additional

work could investigate the different processing options available to achieve ways to produce deep-draw materials.

8. Bibliography

1. Aimone, J., Challenges and Opportunities for Designing and Manufacturing Molded and Needled Automotive Products. Molding and Forming of Polymers Conference. Atlanta, Ga.1985

2. Anton A., Gross, R., The Preparation, Testing and Utilization of High Radial stretch Fabrics for Molding. Molding and Forming of Polymers Conference. Atlanta, Ga.1985

3. Baillargeon, y., Vu-Khanh, T. Prediction of Fiber Orientation and Microstructure of Woven Fabric Composites after Forming. Composite Structures. Volume 53. 2002. p 475

4. Beil, N. B., Roberts, W., Modeling and Computer Simulation of the Compressional Behavior of Fiber Assemblies, Part 1: Comparison to van Wyk's Theory. Textile Research Journal, Volume 72. No. 4 2002. p 341

5. Beil, N. B., Roberts, W., Modeling and Computer Simulation of the Compressional Behavior of Fiber Assemblies, Part II: Hysteresisi, Crimp, and orientation Effects. Textile Research Journal, Volume 75, No. 5, 2002. p 375

6. Benedyk, J. Molding nonwoven, needle Punched fabrics into three-dimensional Shapes. U.S. Patent No 4,258,093 March 24, 1981

7. Bessey, W. Rumierz, G., Felton, C. Rigid fiber network having improved post-Yield Dimensional recovery, Method of making same, and articles incorporating same. U.S. Patent No. 5,851,930 December 22, 1998

8. Bhat, G., Nonwovens as Three-Dimensional Textiles for Composites. Materials and Manufacturing processes. Volume 10, No. 4, p 667, 1995

9. Bigg, D., Jacomet, A. The Effect of the Processing Performance of Thermoplastic Sheet Composites. Molding and Forming of Polymers Conference. Atlanta, Ga.1985

10. Bikales, N., Molding of Plastics. Wiley–Interscience. New York. 1971.

11. Birley, A., Haworth, B., Batchelor, J. Physics of Plastics: Processing, Properties and Materials Engineering. Oxford university Pres. 1991

12. Boisse, p., Gasser, A., Hivet, G. Analyses of Fabrics Tensile behavior: determinations of the biaxial tension-strain surfaces and their use in thermoforming. Composites: Part A. volume 32. 2001, p 1395

13. Brandt, J., Drechlser, K., Arendts, F. Mechanical performance of Composites Based on Various Three-Dimensional Woven, Fiber Preforms. Composites Science and Technology. Volume 56. 1996. p. 381

14. Dessenberger, R., Tucker III, C. Forming Limit Measurements of Random Fiber Mats. Polymer Composites, volume 19, No. 4, August 1998. p. 370 Molding and Forming of Polymers Conference. Atlanta, Ga.1985

15. Disselbeck, D., Network materials: Reinforcing and Stiffening with Three-Dimensional Textile Structures. Journal of Coated Fabrics, Vol. 19. No. 1. 1990. p 193

16. Disselbeck, D., Elke, G., manufacture of a Three-dimensionally Shaped textile material and Use Thereof. U.S. Patent No. 5,364,686 November 5, 1994

17. Dominski, D., Three-dimensional and Formed Fabrics for Construction Applications. Molding and Forming of Polymers Conference. Atlanta, Ga.1985

18. Eisele, D., Bocholt. Flat Nonwovens and Molded Elements for Use as Motor Car Trims. Melliand Textilberichte

19. Florian, J., Practical Thermoforming: Principles and Applications, 2nd Edition. Marcel Dekker, Inc. New york. 1996

20. Ghosh, S., Chapman, L., An Investigation on Needling Parameters of Moldable Nonwoven Fabrics Produced Form Blended Thermoplastic Fibers. International Nonwovens Technical Conference, September 7, 2001, Baltimore, MD

21. Grissett, G., Pourdeyhimi, B. 3D SpaceNet® Structures From Nonwovens. NCRC Industrial Advisory Board Report, November 2000

22. Hofstee, J., de Boer, H., van Keulen, F., Elastic Stiffness analysis of a Thermo-formed plain-Weave Fabrics Composite- part III: Experimental Verification. Composites Science and Technology. Volume 62. 2002. p. 401

23. Holliday, T. Forming and Molding: Three-Dimensional Nonwovens. Nonwovens Industry. Vol. 25, No. 4 p 34

24. Huntoon et al. Ultra Resilient Three Dimensional Nonwoven Fiber material and Process for Making the Same. U.S. Patent No. 5,906,879 May 25, 1999

25. Illig, A. Thermoforming: A Practical Guide. Hanser publishers. New York. 2001

26. Kim, D., Wiley, J., Bessey, W. Thermoplastic Three Dimensional Fiber Network. U.S. Patent No. 6,007,898 December 28, 1999

27. Komori, T., Itoh, M. analyzing the Compressability of a Random Fiber Mass Based on the Modified Theory of Fiber Contact. Textile Research journal. Volume 67. No. 3. 1997. p 204

28. Kotharo, V., Das, A. Compressional Behavior of Nonwoven Geotextiles. Geotextiles and Geomembranes. Volume 11, 1992. p. 235

29. Kotharo, V., Das, A. Compressional Behavior of layered needle-Punched Nonwoven Geotextiles. Geotextiles and Geomembranes. Volume 12, 1993. p. 179

30. Kotharo, V., Das, A. The Compressional Behavior of Spunbonded Nonwoven Fabrics. Journal of the Textile Institute. Volume 84, no. 1, 1993, p. 16

31. Kuyzin. G., Schlotterbeck, D., Kent, G., Low Density SRIM-Non-Glass Reinforced Polymer Composites for Automotive Interior Applications. Journal of Coated Fabrics, Volume 19. April 1990, p. 211

32. Lau, H., Bhattacharya, S., Field, G. Melt Strength of Polypropylene: Its Relevance to Thermoforming. Polymer Engineering and Science. Volume 38, No. 11, November 1998, p 1915

33. Li, y., Yang, S., Kniss, D. Thermal Compression and Characterization of Three-dimensional Nonwoven PET matrices as Tissue Engineering Scaffolds. Biomaterials. Volume 21, p. 609, 2000

34. Lim. T., Ramakrishna, S., Shang, H., Optimization of the Formability of Knitted Fabrics Composite Sheet by Means of Combined Deep Drawing and Stretch Forming. Journal of Materials Processing Technology Volume 89-90. 1999. p. 99

35. Lucca, E., Gillard, P. Method of producing formed Structural Element. U.S. Patent No. 5,160,406 November 3, 1992

36. Machida, T., Lee, D., Deep Drawing of Polypropylene Sheets Under Differential Heating Conditions. Polymer Engineering and Science. Volume 28, no. 7, mid April 1988, p 405

37. Mansfield, R., Automotive Molded Products form Nonwovens. Molding and Forming of Polymers Conference. Atlanta, Ga.1985

38. Margolis, J. Instrumentation for Thermoplastic Engineering. Hanser Publishers. New York. 1988

39. Mascia, L. Thermoplastic Materials Engineering, 2nd Edition. Elsivier Applied Science. London. 1989

40. Mukhopadhyay, S. K., The Structure and Properties of Typical Melt-Spun Fibers. Textile Progress. Volume 18 (4).

41. Nam, G., Ahn, K., Lee, J. Three-Dimensional Simulation of Thermoforming Process and Its Comparison with Experiments. Polymer Engineering and Science. Volume 40, No. 10, October 2000, p 2232

42. Nicholls, R., Nonwovens as Reinforcement for Construction Products. Molding and Forming of Polymers Conference. Atlanta, Ga.1985

43. Pede, S. Woodhams, R. Deep Drawing of Self-Reinforced Thermoplastic Sheets. Polymer Engineering and Science. Volume 30 No. 19. 1990 p. 1185

44. Pegoretti, A., Marchi, A., Riccò. Determination of the Fracture Toughness of Thermformed Polypropylene Cups by Essential Work Method. Polymer Engineering and Science. Volume 37, No. 6, June1997. p. 1045

45. Potluri, P., Porat., Sharma, S. Three Dimensional Weaving and Molding of Textile Composites.

46. Rozant, O., Bourban,P., Månson, J., Warp-knit Laminates for Stampable sandwich Preforms. Composites Science and Technology. Volume 61. 2001. p 145

47. Schoppee, M. A Poisson Model of Nonwoven Fiber Assemblies in Compression at High Stress. Textile Research journal. Volume 68, No. 5, 1998. p 371.

48. Segawa, Y., Saiki, N. Fibrous Shaped Articles having Non-level Surface U.S. Patent No. 4,242,398 December 30, 1980,

49. Thornton, D., Clarke, R. Thermally Formed Filter. U.S. Patent No. 4,772,443 September 20, 1988

50. Throne, J. Technology of Thermoforming. Hanser Publishers. New York. 1996.

51. Throne, J. Understanding Thermoforming. Hanser Publishers. New York. 1999.

52. Throne, J. Thermoforming. Hanser Publishers. New York. 1987.

53. Twilley, I., Farley, R. Method of Manufacturing Molded Articles. U.S. Patent No. 4,869,855 September 26, 1989

54. Ugbolue, S.C. Structure/property Relationships in Textile Fibers. Textile Progress. Volume 20 (4)

55. Velu, y., Farer, R., Chodh, T., Seyam, A. Formations of Shaped/Molded Meltblowing Nonwoven Structures. Journal of Textile and Apparel, Technology and Management. Volume 1 (1). September 2000

56. Watanbe, A., Miwa, M., Yokoi, T., Fatigue Behavior of Aramid Nonwoven Fabrics Under Hot-Press Conditions Part VI: Effect of Stable Base Fabrics on Mechanical Properties. Textile Research journal. Volume 69. No. 1. 1999. p 1.

57. Wulfhorst, B., Büsgen, A., Weber, M., Three-Dimensional Textile Intermediate Products for the Economical Manufacturing of Construction Elements Made form Fiber Composite Materials. Melliand Textilberichte. 71(1990), p. 672

58. Xue,p., Yu,T., Tao, X., Energy-Absorbing Capacity of Grid-Domed Textile Composites. Composites Science and Technology. Volume 60. 2000. p 785

59. Xue,p., Yu,T., Tao, X., Effect of Cell Geometry on the Energy-Absorbing Capacity of Grid-Domed Textile Composites. Composites: Part A. Volume 31. 2001. p. 861

60. Yu, J.., Formability of Textile Performs for Composite Applications. Part 1: Characterization Experiments. Composites Manufacturing. Masters Thesis. Drexler University

61. Yu, J., Cai, Z., Ko, F., Formability of Textile Performs for Composite Applications. Part 1: Characterization Experiments. Composites Manufacturing. Vol. F (2) 1994. p. 113.

62. Yu, J., Cai, Z., Ko, F., Formability of Textile Performs for Composite Applications. Part 2: Evaluation Experiments and Modeling. Composites Manufacturing. Vol. F (2) 1994. p. 123.

63. ASTM Standard Test Method 5035-95: Breaking Force and Elongations of textile Fabrics (Strip Method)

64. Structures Via Binder Fibers and Powders. Molding and Forming of Polymers Conference. Atlanta, Ga.1985

65. Molding of Industrial Products. Molding and Forming of Polymers Conference. Atlanta, Ga.1985

66. Lightweight Three-Dimensional Structures. High Performance Textiles. September 1999. p. 5.

67. Creating Three-Dimensional Nonwovens. Technical Textiles International. July/august 1998 p 6.

68. Polyester Nonwovens for Car Interior Trim. ITB Nonwovens: Industrial Textiles. Volume 4 1997, p 12

69. Molding opens New Vistas for nonwovens. Textile World. August 1986. p. 75.

70. Keeping it in- The Future for Closed Mold Processes. Reinforced Plastics, February 2000. p. 32

71. ASTM-D5733-99 Standard Test Method for Tearing strength of Nonwoven Fabrics by the Trapezoid Procedure

72. ASTM Standard Test Method 6272-00: Standard test method for Flexural properties of Unreinforced and Reinforced Plastics and electrical Insulating Materials by Four Point Bending.

9. Appendices

9.1 Appendix A: Draw Ratio

Several assumptions for calculating draw-ratio were made. First, a perfect grid of "domes" or frustums of right circular cones normal to the substrate plane describes the geometric shape produced utilizing male/female mold geometry on the SpaceNet system (refer to figure 1.1). Secondly, a finite initial surface area is provided in which the final surface area is produced. This has the implication of selecting an initial surface area to base draw-ratio calculations on. As described in the current report, draw ratio (DR) is given by:

$$DR = \frac{A_{SF}}{A_I}$$

Where the initial surface area (A_I) is the pre-molding area and the final surface area (A_{SF}) is the increase in surface area achieved post molding.

Consider the unit cell of a grid-domed structure proposed in this thesis;

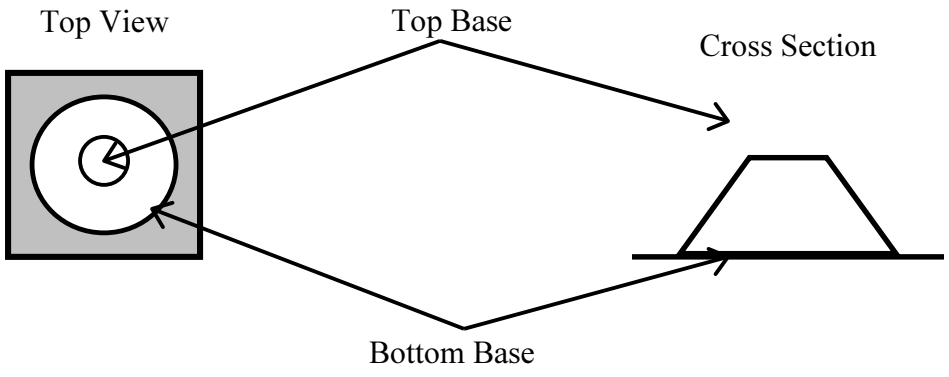

Within a unit cell, the final surface area (A_F) is comprised of the lateral surface area (L) of the frustum, the area of the top base (A_t), and the difference of the initial surface area (A_I) the area of the bottom base (A_b), and is given by:

$$A_{SF} = [a(L) + a(A_t)] + [(A_I) - a(A_b)] \; * \qquad (1)$$

Where a, is the total number of domes in a give area, in the unit cell $a=1$. Is governed by the male pin diameter female hole diameter.

To establish the lateral surface area of a frustum, consider a Frustum of a Right Circular Cone:

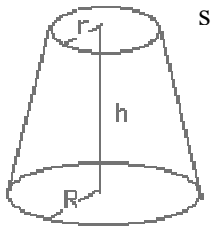

http://mathworld.wolfram.com/ConicalFrustum.html

Which is comprised of a Height (h) a top base radius (r) a bottom base radius (R) and a slant height (s). Slant height (s) is given by:

$$s = \sqrt{([R-r]^2 + h^2)} \qquad (2),$$

The lateral surface area (L) of the frustum is given by:

$$L = \pi(r+R)s \qquad (3),$$

Area of top base (A_t) :

$$A_t = \pi r^2 \qquad (4),$$

Area of Bottom base (A_b):

$$A_b = \pi R^2 \qquad (5),$$

Inserting equation 3, 4 and 5 in equation 1 provides the final surface area

$$A_{SF} = [a(\pi(r+R)s) + a(\pi r^2)] + [(A_I) - a(\pi R^2)] \ , \qquad (6)$$

A_I = *initial surface area*

Example 1 Calculation of Draw ratio:

Consider a three-dimensional structure described in this report with an initial length and width of 101.6 mm. Utilizing a 9.525 mm (3/8") male pin diameter in conjunction with a 15.875 mm (5/8") female hole. The following parameters come forth:

Length (L_I), mm	**101.6**
Width (W_I), mm	**101.6**
# of "Domes"	**16**
Radius @ Dome Base, mm	**7.9375**
Radius @ Dome Top, mm	**4.7625**
Dome Height (h), mm	**12**

$$DR = \frac{A_{SF}}{A_I} = \frac{12639.849 mm^2}{10322.56 mm^2} = 1.222$$

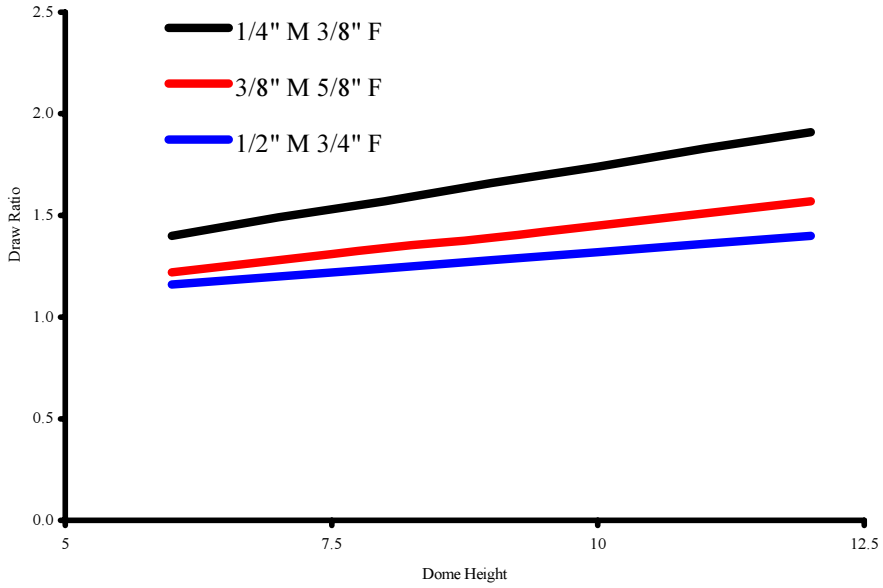

Figure A.1 Draw Ratio and Product Thickness

9.2 Appendix B: Calculation of Standard Errors

From the Full Model

Whole Plot Error: $\sigma_\delta^2 = 0.03906$

Sub-Plot Error: $\sigma_\varepsilon^2 = 0.1136$

t=3, m=2, r=3

Temperature Means

$\text{Var}(Y_{0..}) = \text{Var}(\sigma_\delta^2/m + \sigma_\varepsilon^2/mr) = \text{Var}(\sigma_\delta^2/2 + \sigma_\varepsilon^2/6)$

$\text{Var}(Y_{1..}) = \text{Var}(\sigma_\delta^2/m + \sigma_\varepsilon^2/mr) = \text{Var}(\sigma_\delta^2/2 + \sigma_\varepsilon^2/6)$

$\text{Var}(Y_{2..}) = \text{Var}(\sigma_\delta^2/m + \sigma_\varepsilon^2/mr) = \text{Var}(\sigma_\delta^2/2 + \sigma_\varepsilon^2/6)$

Or generally,

$\text{Var}(Y_{i..}) = \text{Var}(\sigma_\delta^2/m + \sigma_\varepsilon^2/mr) = \text{Var}(\sigma_\delta^2/2 + \sigma_\varepsilon^2/6)$

$SE(Y_{i..}) = \text{Sqrt}(\sigma_\delta^2/m + \sigma_\varepsilon^2/mr) = \text{Sqrt}(0.03906/2 + 0.1136/6) = 0.1961$

Residence Time Means

$\text{Var}(Y_{..0}) = \text{Var}(\sigma_\delta^2/mt) + \text{Var}(\sigma_\varepsilon^2/tm) = \sigma_\delta^2/6 + \sigma_\varepsilon^2/6$

$\text{Var}(Y_{..1}) = \text{Var}(\sigma_\delta^2/mt) + \text{Var}(\sigma_\varepsilon^2/tm) = \sigma_\delta^2/6 + \sigma_\varepsilon^2/6$

$\text{Var}(Y_{..2}) = \text{Var}(\sigma_\delta^2/mt) + \text{Var}(\sigma_\varepsilon^2/tm) = \sigma_\delta^2/6 + \sigma_\varepsilon^2/6$

Or generally,

$\text{Var}(Y_{..k}) = \text{Var}(\sigma_\varepsilon^2/tm) + \text{Var}(\sigma_\delta^2/mt) = \sigma_\varepsilon^2/6 + \sigma_\delta^2/6$

$SE(Y_{..k}) = \text{Sqrt}(\sigma_\delta^2/6 + \sigma_\varepsilon^2/6) = \text{Sqrt}(0.03906/6 + 0.1136/6) = 0.1595$

9.3 Appendix C: Test for Normality Compressive Stress & Energy

9.3.1 Compressive Stress

Residual Vs. Predicated

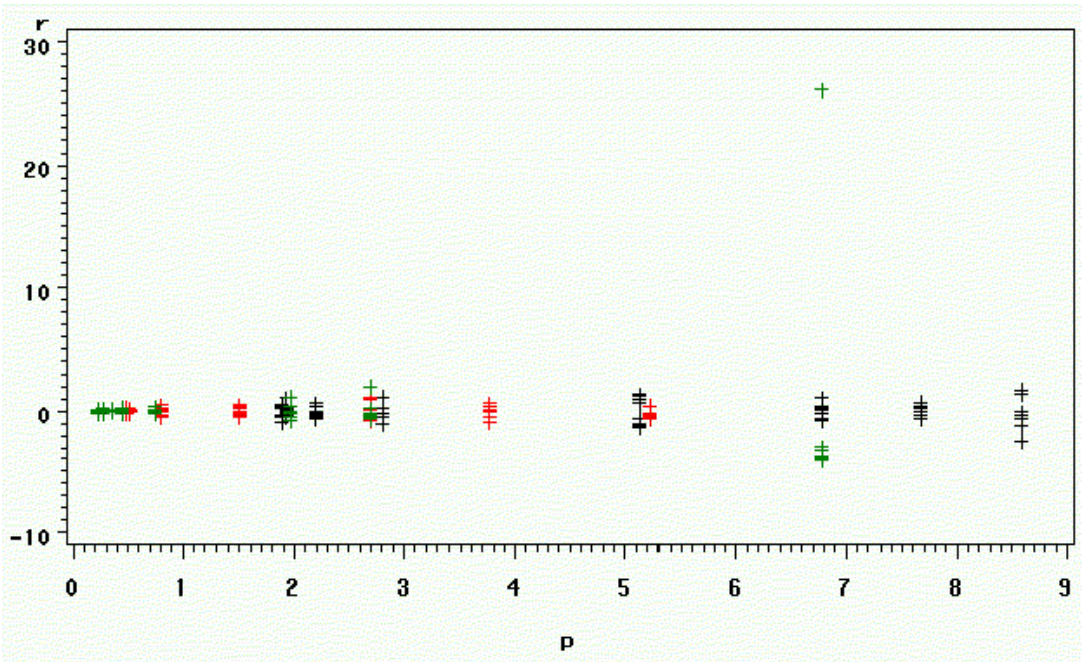

Normal Probability Plot ¼" Pin Diameter

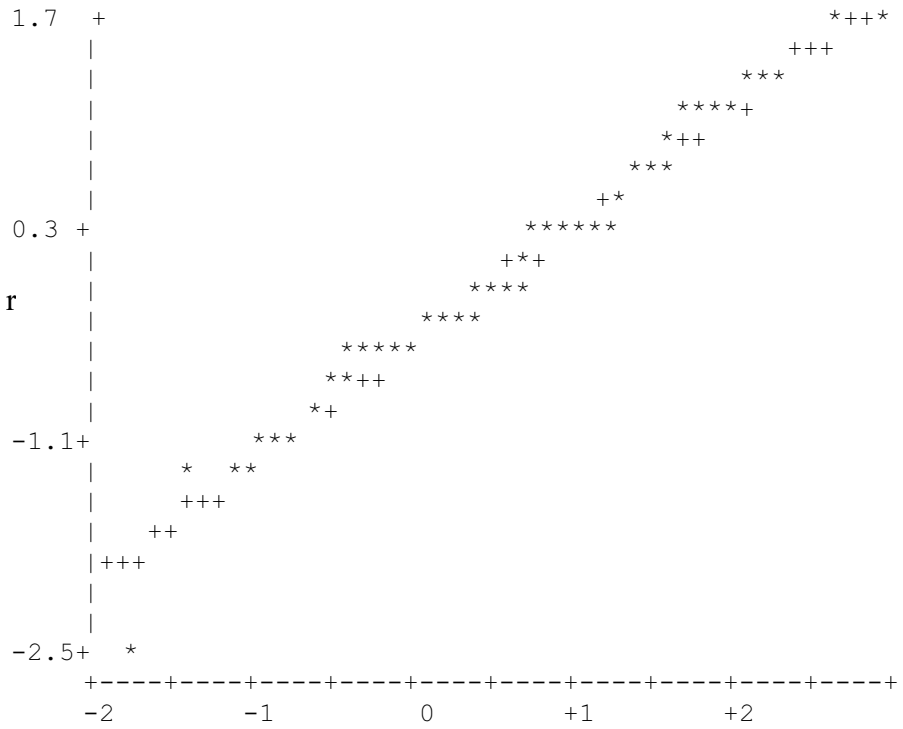

Normal Probability Plot 3/8” Pin Diameter

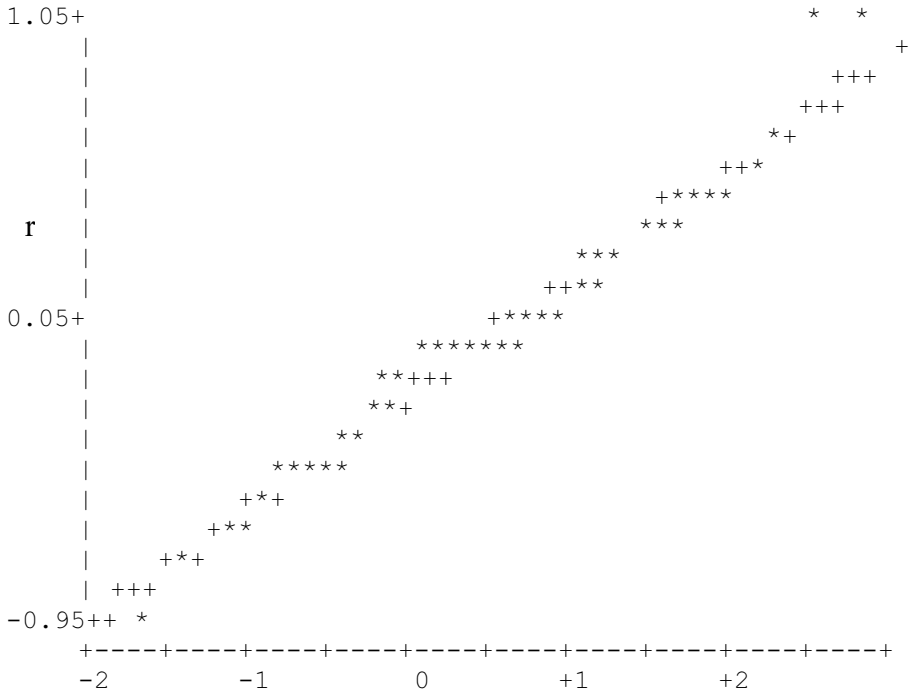

Normal Probability Plot ½” Pin Diameter

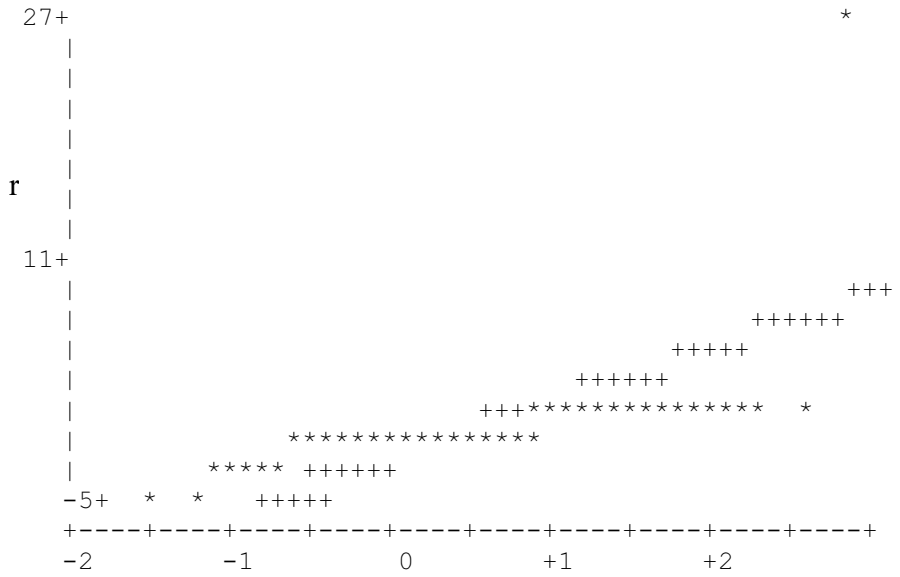

9.3.2 Compressive Secant Modulus

Residuals Vs. Predicted

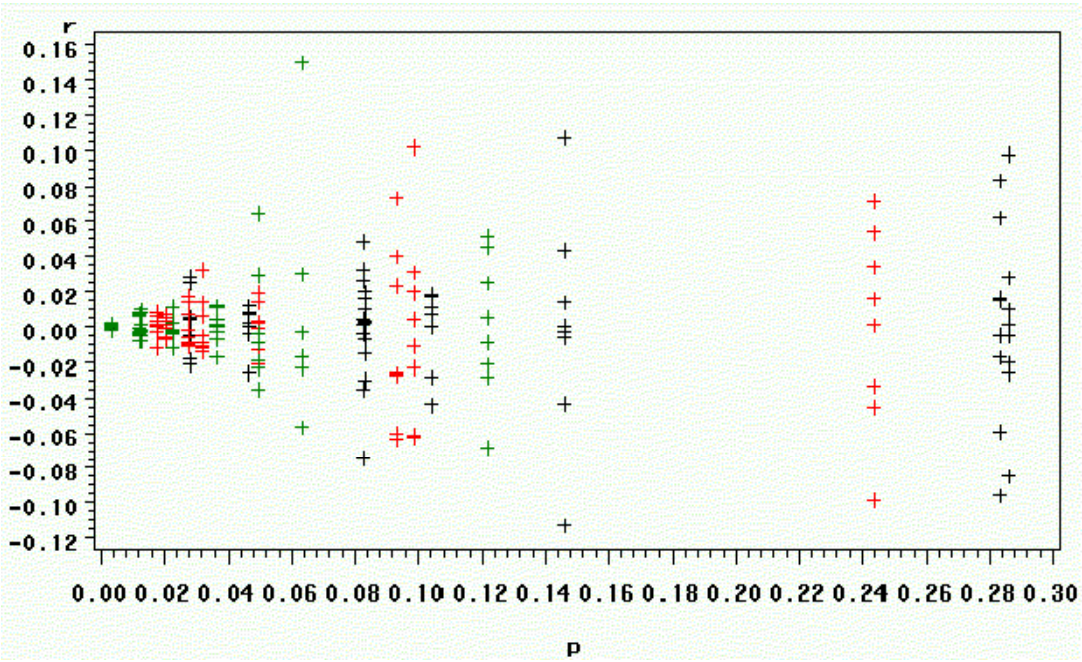

Normal Probability Plot ¼" Pin diameter

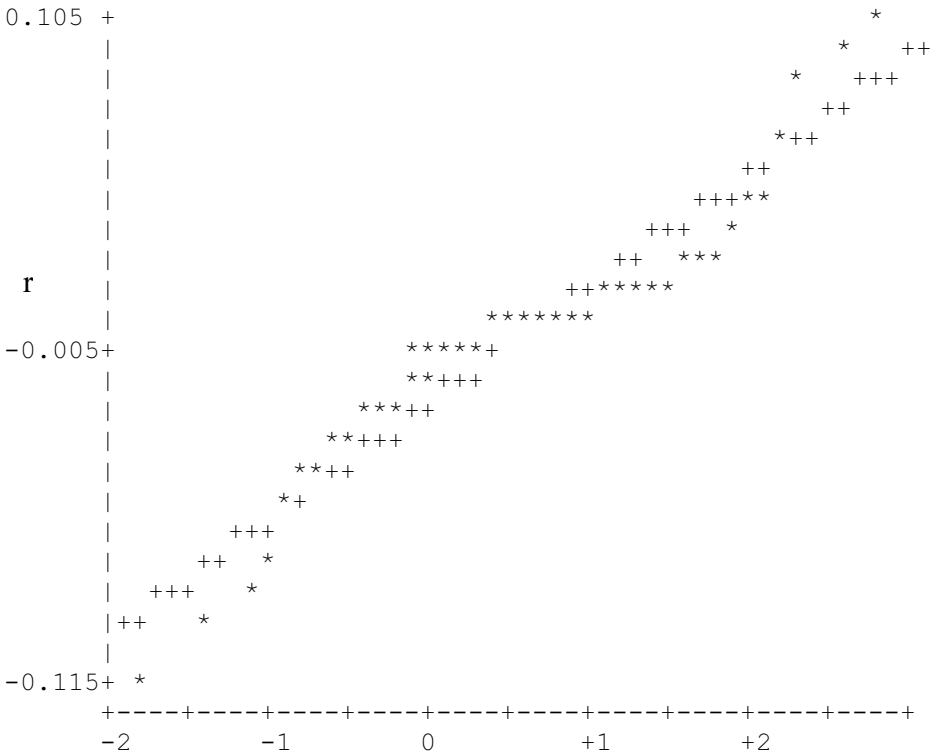

Normal Probability Plot 3/8" Pin Diameter

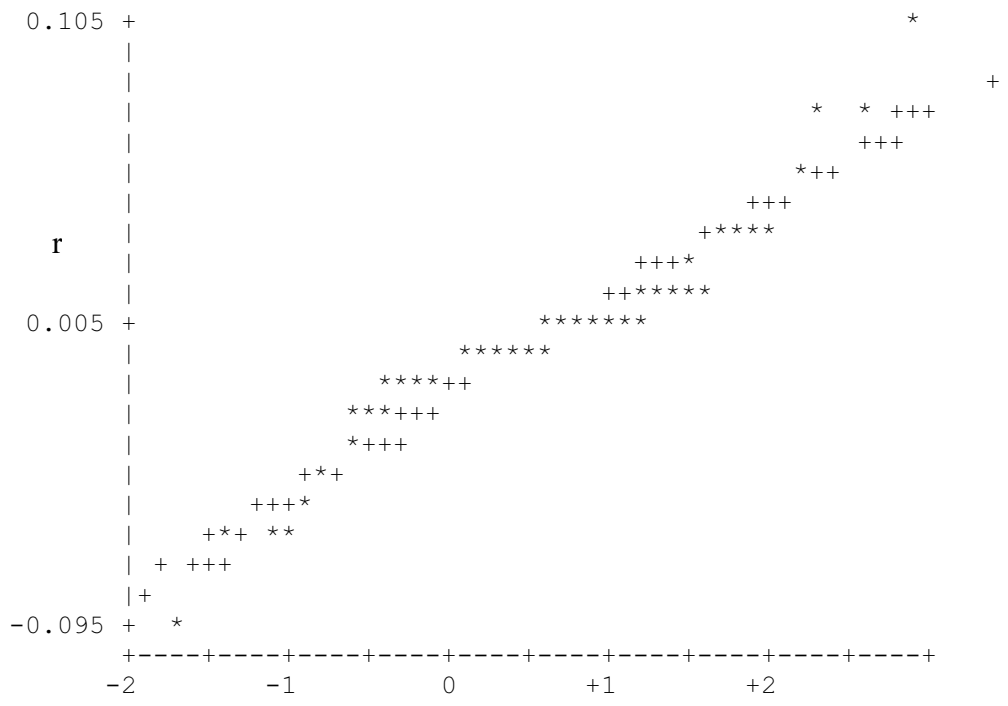

Normal Probability Plot ½" Pin Diameter

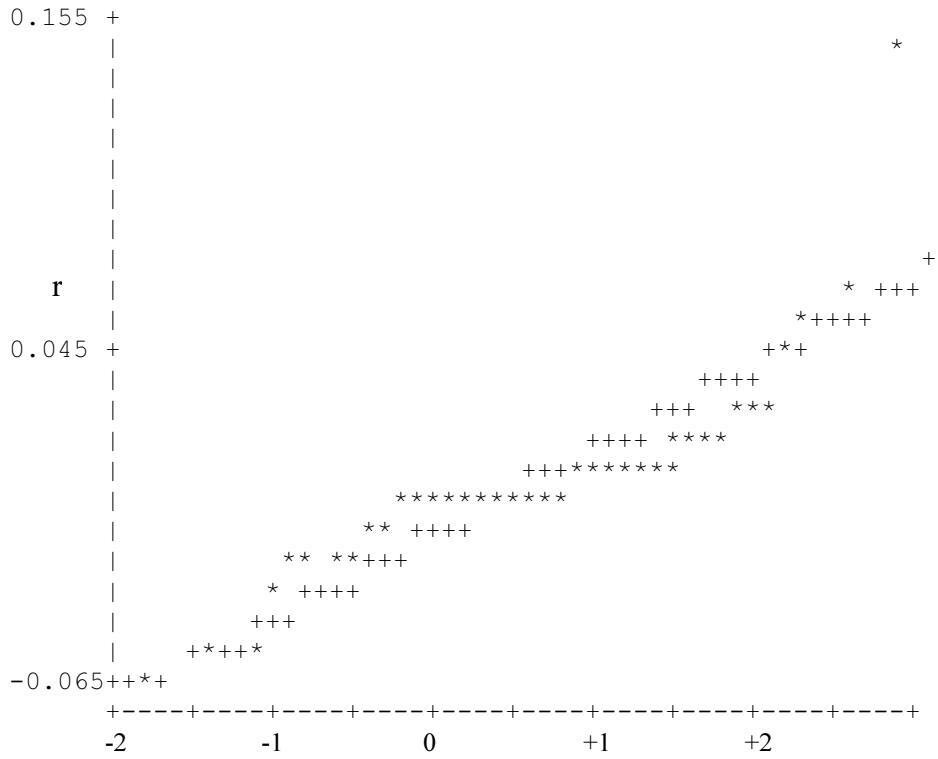

9.4 Appendix D: Compressive Energy Data

Table 1.Total Energy to 40% Strain (kj/m^2)

	1/4"	3/8"	1/2"
52-100	271.82	68.6	43.29
52-140	432.64	131.827	80.23
52-180	693.957	243.916	151.17
56-130	306.47	89.63	56.33
72-100	354.218	95.49	58.5
72-180	1212.78	420.235	280.96
2295	1327.24	656.38	477.97
2033	1087.12	541.95	448.159

Table 3. Hysteresis (kj/m2)

	1/4"	3/8"	1/2"
52-100	120.37	17.78	24.64
52-140	273.8	55.98	59.95
52-180	365.7	136.34	84.11
56-130	143.4	35.6	21.3
72-100	124.7	47.63	27.26
72-180	832.56	233.1	155.48
2295	1002.16	453.24	326.80
2033	814.9	330.97	326.10

Table 2. Recovered Energy (kj/m^2)

	1/4"	3/8"	1/2"
52-100	151.45	50.82	18.65
52-140	158.84	55.85	20.27
52-180	328.25	107.57	67.05
56-130	163.07	54.03	35.03
72-100	229.52	47.86	31.23
72-180	380.22	187.15	125.48
2295	325.08	203.14	151.17
2033	272.22	210.98	122.04

Table 4.Hysteresis as a % of Total Energy

	1/4"	3/8"	1/2"
52-100	44.28	25.91	56.92
52-140	63.28	42.46	74.72
52-180	52.69	55.89	55.64
56-130	46.79	39.72	37.82
72-100	35.2	49.83	46.59
72-180	68.65	55.47	55.34
2295	75.5	69.05	68.37
2033	74.95	61.07	72.76

Table 5. Substrate Tear Strength

Substrate	Machine Direction	Standard Deviation	Cross Direction	Standard Deviation
52-100	17.60331	6.076331	22.44383	2.910483
52-140	27.58326	3.031583	27.35858	4.030174
52-180	39.96208	4.849669	39.59346	2.932114
72-100	11.06104	2.295091	13.309	1.569161
72-180	25.71148	1.79067	28.11821	3.086455
56-130	21.77991	2.775918	21.56974	1.843025
2295	9.5067	1.865522	8.764157	1.655027
2033	6.675329	1.2449	8.694454	1.285021
SF 27	20.59076	3.672732	21.63128	2.748107
SF 44	36.65065	5.586376	37.23353	7.481403
SF 94	55.81351	15.75184	63.56304	10.47472
PGI T	23.92967	1.757634	21.43268	2.759306
PGI H	19.4072	2.345184	18.35167	1.946319

Table 6. Substrate Flexural Strength

Substrate	Machine Direction	Standard Deviation	Cross Direction	Standard Deviation
52-100	0.1912735	0.0527656	0.123661	0.036247
52-140	0.2837966	0.0527489	0.241538	0.046891
52-180	0.5827171	0.0916905	0.469732	0.080811
75-100	0.1868253	0.916665	0.152574	0.039844
72-180	0.3643094	0.0756183	0.383437	0.051611
56-130	0.3212728	0.0687365	0.299766	0.055068
2295	0.3353959	0.0482381	0.364754	0.06001
2003	0.4417084	0.123434	0.280238	0.088593
SF 27	0.4288086	0.086477	0.208177	0.053799
SF 44	0.5764896	0.158933	0.355413	0.082354
SF 94	5.2506812	0.898157	2.200091	0.3000775
PGI-T	0.1659187	0.0224918	0.165919	0.022492
PGI-H	0.139889	0.0184661	0.13989	0.018466

9.5 Appendix E: Regression Analysis removing SF-94 from Data Set

As described in Chapter 4, it was hypothesized the compressive stress is associated with several substrate characteristics including basis weight and the "level of bonding". The compressive stress of all formed products (y, or dependent variable) was regressed against independent variables: substrate tear strength (x_1), flexural strength (x_2), and basis weight. (x_3). Note that one replicate was used thus providing the following (full) linear model:

$$Y_i = \beta_0 + \beta_1 x_{i1} + \beta_2 x_{i2} + \beta_3 x_{i3} + \varepsilon_i$$

β_0, β_1, β_2, β_3 are all regression parameters

Where i =1 to *n*

$\varepsilon_i \sim N(0, \sigma^2)$.

Iid

Where Y_i represents the mean compressive stress for a given tear strength (x_1), flexural strength (x_2), and basis weight. (x_3). While strong Pearson correlation coefficients were observed between the compressive stress of all formed products (y, or dependent variable) and all independent variables: substrate tear strength (x_1), flexural strength (x_2), and basis weight (x_3). However, multiple linear regression revealed that only flexural strength (x_2) showed a linear association with compressive stress (y) with 95-% confidence. Observing substrate properties it was observed that the SF-94 substrate displayed the largest flexural strength relative to the remaining substrates. It can be surmised that the magnitude of flexural strength and compressive stress for SF 94 relative to other a substrates contributed greatly to the strong Pearson correlation coefficients observed (refer to figures 4.11 and 4.14, Tables 4.8 and 4.9). Multicollinearity among independent variables therefore affected multiple linear regression output.

To understand the extent of how multicollinearity among independent variables in the previously described regression analysis, SF 94 was removed from the data set and multiple linear regression was completed (including Pearson correlation coefficients). Table 1 displays the partial estimated regression coefficients with SF-94 removed from the data set for the regression model proposed.

Flexural strength (β_3), Tear strength (β_1) and basis weight (β_2), do not display a linear association with compressive stress based on the partial estimated regression coefficients (p=0.32, p= 0.53 and p=0.80), respectively. Table 2 reports correlation coefficients of –0.24 and –0.17 for tear strength and basis weight, respectively. A correlation coefficient of 0.5734 was observed between flexural strength and compressive stress. While flexural strength still reports the highest correlation observe a *strong* linear association between flexural strength and compressive stress cannot be concluded when SF 94 is removed from the data set.

Table 1 Regression Coefficients without SF-94 in data set

Parameter	Estimate	Standard Error	t Value	P-Value
Intercept	1.90019	2.306994	0.82	0.4967
Tear Strength	-0.0455	0.06169	-0.74	0.5376
Flexural Strength	5.417241	4.223898	1.28	0.3282
Basis Weight	0.005214	0.018562	0.28	0.805

Table 2 Pearson Correlation Coefficients without SF-94 in data set

	Compressive Stress	Tear Strength	Flexural Strength	Basis Weight
Compressive Stress	1.00000	0.24211	0.5734	-0.17454
Tear Strength	-0.24211	1	0.20504	0.59972
Flexural Strength	0.5734	0.20504	1	-0.091
Basis Weight	-0.17454	0.59972	-0.091	1